Supplementary material

Novel multi-material photo-curable resins containing high-performance photoinitiating systems and nano additives dedicated to 3D-VAT printing.

Magdalena Jankowska[a], Anna Chachaj-Brekiesz[b], Klaudia Trembecka-Wójciga[c], Anna Jarzębska[c], Monika Topa-Skwarczyńska[a], Maciej Pilch[a], Joanna Ortyl[a, d, e]

[a] Department of Biotechnology and Physical Chemistry, Faculty of Chemical Engineering and Technology, Cracow University of Technology, Warszawska 24, 30-155 Cracow, Poland

[b] Faculty of Chemistry, Jagiellonian University, Gronostajowa 2, 30-387 Cracow, Poland

[c] Institute of Metallurgy and Materials Science, Polish Academy of Sciences, Reymonta 25, Cracow, Poland

[d] Photo4Chem Lea 114, 30-133 Cracow, Poland

[e] Photo HiTech Ltd., Bobrzynskiego 14, 30-348 Cracow, Poland

* Correspondence: jortyl@pk.edu.pl

CONTENTS

Synthesis of 9-[(E)-2-phenylethenyl]anthracene and 9-[(E)-2-phenylethenyl]phenanthrene derivatives

Synthetic methods

9-[(E)-2-phenylethenyl]anthracene and 9-[(E)-2-phenylethenyl]phenanthrene derivatives were synthesized via Heck coupling of 9-bromoanthracene or 9-bromophenanthrene with an appropriate styrene derivative. As the obtained compounds were already described in the literature the structure of products was confirmed solely by NMR analysis. ^{1}H NMR spectra were recorded in DMSO-D_6 or $CDCl_3$ on Advance III HD 400 MHz (Bruker) spectrometer. Chemical shifts are reported in parts per million (δ) and were referenced to residual protonated solvent peak (δ = 2.50 ppm for DMSO-D_6 or δ = 7.26 ppm for $CDCl_3$). All organic compounds, inorganic salts and solvents were analytically pure and used as received. DMF was dried over molecular sieves.

Procedure for synthesis of 9-[(E)-2-phenylethenyl]anthracene and 9-[(E)-2-phenylethenyl]phenanthrene derivatives

9-bromoanthracene or 9-bromophenanthrene (257 mg, 1.00 mmol), appropriate derivative of styrene (1.20 mmol), triphenylphosphine (20 mg, 0.07 mmol), palladium(II) acetate (18 mg, 0.08 mmol), potassium carbonate (363 mg, 2.63 mmol) and dry DMF (5.0 cm^3) were placed in the pressure vial under nitrogen. The mixture was stirred and heated in temperature 100 °C for 24 h. After cooling water (20 cm^3) was added and resulting mixture was extracted with chloroform (3 x 15 cm^3). Chloroform extracts were combined, washed with water and brine, dried over anhydrous magnesium sulfate and concentrated under vacuum. The oily residue was adsorbed on silica gel and purified by column chromatography on silica gel using eluent gradient (hexanes→chloroform).

Physicochemical data for studied 9-[(E)-2-phenylethenyl]anthracene and 9-[(E)-2-phenylethenyl]phenanthrene derivatives

Structure	
9-[(E)-2-phenylethenyl]anthracene[1–3], **ANT-H**	
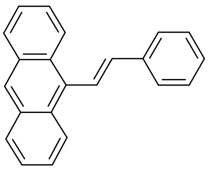	Synthesized from 9-bromoanthracene (257 mg, 1.00 mmol) and styrene (0.125 mg, 1.20 mmol) in 83% yield. **^{1}H NMR (400 MHz, $CDCl_3$) δ [ppm]:** 8.42 (s, 1H), 8.39 – 8.34 (m, 2H), 8.06 – 8.00 (m, 2H), 7.93 (dd, J = 16.5, 0.6 Hz, 1H), 7.72 – 7.67 (m, 2H), 7.53 – 7.42 (m, 6H), 7.37 (m, 1H), 6.96 (d, J = 16.6 Hz, 1H)
9-[(E)-2-(4-cyanophenyl)ethenyl]anthracene[3–5], **ANT-CN**	
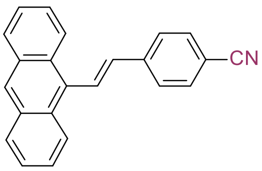	Synthesized from 9-bromoanthracene (257 mg, 1.00 mmol) and 4-cyanostyrene (0.155 mg, 1.20 mmol) in 85% yield. **^{1}H NMR (400 MHz, DMSO) δ [ppm]:** 8.60 (s, 1H), 8.41 – 8.29 (m, 3H), 8.12 (dd, J = 6.4, 3.4 Hz, 2H), 8.05-8.00 (m, 2H), 7.95-7.89 (m, 2H), 7.58 – 7.52 (m, 4H), 7.08 (d, J = 16.6 Hz, 1H)
9-[(E)-2-[4-(methylsulfanyl)phenyl]ethenyl]anthracene, **ANT-SCH_3**	
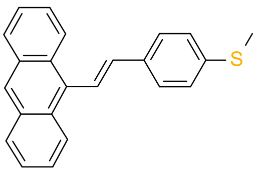	Synthesized from 9-bromoanthracene (257 mg, 1.00 mmol) and 4-(methylsulfanyl)styrene (0.180 mg, 1.20 mmol) in 96% yield. **^{1}H NMR (400 MHz, DMSO) δ [ppm]:** 8.58 (s, 1H), 8.38 – 8.30 (m, 2H), 8.13 – 8.04 (m, 3H), 7.80-7.74 (m, 2H), 7.56 – 7.50 (m, 4H), 7.39-7.34 (m, 2H), 6.94 (d, J = 16.6 Hz, 1H), 2.55 (s, 3H)
9-[(E)-2-([1,1'-biphenyl]-4-yl)ethenyl]anthracene, **ANT-C_6H_5**	
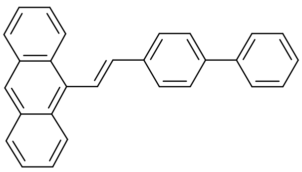	Synthesized from 9-bromoanthracene (257 mg, 1.00 mmol) and 4-phenylstyrene (0.216 mg, 1.20 mmol) in 65% yield. **^{1}H NMR (400 MHz, DMSO) δ [ppm]:** 8.61 (s, 1H), 8.43 – 8.36 (m, 2H), 8.21 (d, *J* = 16.6 Hz, 1H), 8.18 – 8.12 (m, 2H), 7.97 – 7.91 (m, 2H), 7.84 – 7.75 (m, 4H), 7.62 – 7.50 (m, 6H), 7.46 – 7.39 (m, 1H), 7.04 (d, *J* = 16.6 Hz, 1H).
9-[(E)-2-(4-methylphenyl)ethenyl]anthracene[5], **ANT-CH_3**	
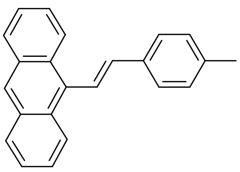	Synthesized from 9-bromoanthracene (257 mg, 1.00 mmol) and 4-methylstyrene (0.142 mg, 1.20 mmol) in 98% yield. **^{1}H NMR (400 MHz, DMSO) δ [ppm]:** 8.58 (s, 1H), 8.39 – 8.32 (m, 2H), 8.16 – 8.10 (m, 2H), 8.06 (d, *J* = 16.6 Hz, 1H), 7.75 – 7.68 (m, 2H), 7.60 – 7.51 (m, 4H), 7.34 – 7.26 (m, 2H), 6.93 (d, *J* = 16.6 Hz, 1H), 2.39 (s, 3H).
9-[(E)-2-(4-methoxyphenyl)ethenyl]anthracene[5], **ANT-OCH_3**	
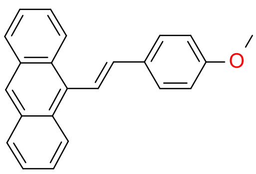	Synthesized from 9-bromoanthracene (257 mg, 1.00 mmol) and 4-methoxystyrene (0.161 mg, 1.20 mmol) in 97% yield. **^{1}H NMR (400 MHz, DMSO) δ [ppm]:** 8.57 (s, 1H), 8.40 – 8.33 (m, 2H), 8.15 – 8.10 (m, 2H), 7.97 (d, *J* = 16.6 Hz, 1H), 7.79 – 7.74 (m, 2H), 7.59 – 7.52 (m, 4H), 7.08 – 7.02 (m, 2H), 6.92 (d, *J* = 16.6 Hz, 1H), 3.84 (s, 3H).
9-[(E)-2-(2-pyridyl)ethenyl]anthracene[6], **ANT-PYR**	
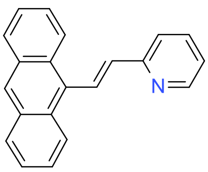	Synthesized from 9-bromoanthracene (257 mg, 1.00 mmol) and 2-vinylpyridine (0.158 mg, 1.20 mmol) in 93% yield. **^{1}H NMR (400 MHz, DMSO) δ [ppm]:** 8.74 – 8.69 (m, 1H), 8.62 (s, 1H), 8.57 (d, *J* = 16.4 Hz, 1H), 8.38 – 8.32 (m, 2H), 8.17 – 8.11 (m, 2H), 7.92 – 7.86 (m, 1H), 7.80 – 7.74 (m, 1H), 7.60 – 7.54 (m, 4H), 7.38 (ddd, *J* = 7.5, 4.8, 1.0 Hz, 1H), 7.10 (d, *J* = 16.3 Hz, 1H).
9-[(E)-2-(4-chlorophenyl)ethenyl]anthracene[7], **ANT-Cl**	

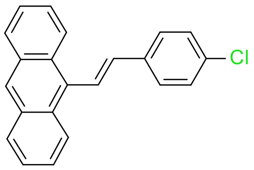	Synthesized from 9-bromoanthracene (257 mg, 1.00 mmol) and 4-chlorostyrene (0.167 mg, 1.20 mmol) in 87% yield. **^{1}H NMR (400 MHz, DMSO) δ [ppm]:** 8.60 (s, 1H), 8.38 – 8.32 (m, 2H), 8.21 – 8.10 (m, 3H), 7.90 – 7.84 (m, 2H), 7.61 – 7.48 (m, 6H), 6.99 (d, *J* = 16.6 Hz, 1H).
9-[(E)-2-(4-fluorophenyl)ethenyl]anthracene, ANT-F	
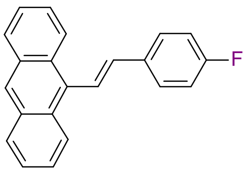	Synthesized from 9-bromoanthracene (257 mg, 1.00 mmol) and 4-fluorostyrene (0.146 mg, 1.20 mmol) in 60% yield. **^{1}H NMR (400 MHz, DMSO) δ [ppm]:** 8.60 (s, 1H), 8.39 – 8.33 (m, 2H), 8.16 – 8.06 (m, 3H), 7.93 – 7.86 (m, 2H), 7.59 – 7.53 (m, 4H), 7.34 – 7.29 (m, 2H), 6.99 (d, *J* = 16.6 Hz, 1H).
9-[(E)-2-phenylethenyl] phenanthrene[8], FEN-H	
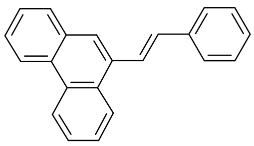	Synthesized from 9-bromophenanthrene (257 mg, 1.00 mmol) and styrene (0.125 mg, 1.20 mmol) in 80% yield. **^{1}H NMR (400 MHz, CDCl$_3$) δ [ppm]:** 8.78 – 8.74 (m, 1H), 8.71 – 8.66 (m, 1H), 8.30 – 8.25 (m, 1H), 7.98 (s, 1H), 7.95 – 7.91 (m, 1H), 7.89 (d, *J* = 15.9 Hz, 1H), 7.74 – 7.58 (m, 6H), 7.47 – 7.40 (m, 2H), 7.36 – 7.31 (m, 1H), 7.24 (d, *J* = 15.9 Hz, 1H).
9-[(E)-2-(4-cyanophenyl)ethenyl]phenanthrene, FEN-CN	
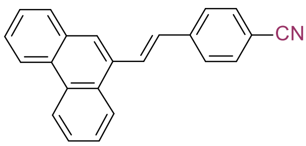	Synthesized from 9-bromophenanthrene (257 mg, 1.00 mmol) and 4-cyanostyrene (0.155 mg, 1.20 mmol) in 90% yield. **^{1}H NMR (400 MHz, DMSO) δ [ppm]:** 8.95 – 8.88 (m, 1H), 8.87 – 8.80 (m, 1H), 8.52 – 8.46 (m, 1H), 8.32 (dd, *J* = 16.0, 6.0 Hz, 1H), 8.28 – 8.23 (m, 1H), 8.09 – 7.99 (m, 3H), 7.93 – 7.86 (m, 2H), 7.81 – 7.64 (m, 4H), 7.48 (dd, *J* = 16.0, 5.8 Hz, 1H).
9-[(E)-2-[4-(methylsulfanyl)phenyl]ethenyl]phenanthrene, FEN-SCH$_3$	
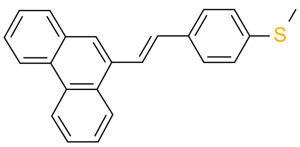	Synthesized from 9-bromophenanthrene (257 mg, 1.00 mmol) and 4-(methylsulfanyl)styrene (0.180 mg, 1.20 mmol) in 96% yield. **^{1}H NMR (400 MHz, DMSO) δ [ppm]:** 8.93 – 8.87 (m, 1H), 8.85 – 8.79 (m, 1H), 8.49 – 8.43 (m, 1H), 8.19 (s, 1H), 8.10 – 8.02 (m, 2H), 7.79 – 7.72 (m, 4H), 7.71 – 7.65 (m, 2H), 7.40 – 7.30 (m, 3H), 2.54 (s, 3H).
9-[(E)-2-([1,1'-biphenyl]-4-yl)ethenyl]phenanthrene, FEN-C$_6$H$_5$	
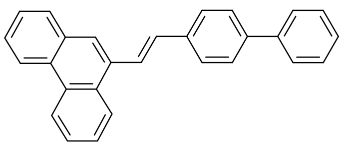	Synthesized from 9-bromoanthracene (257 mg, 1.00 mmol) and 4-phenylstyrene (0.216 mg, 1.20 mmol) in 61% yield. **^{1}H NMR (400 MHz, DMSO) δ [ppm]:** 8.97 – 8.90 (m, 1H), 8.89 – 8.81 (m, 1H), 8.55 – 8.47 (m, 1H), 8.24 (s, 1H), 8.17 (d, *J* = 16.0 Hz, 1H), 8.11 – 8.04 (m, 1H), 7.96 – 7.89 (m, 2H), 7.80 – 7.66 (m, 8H), 7.54 – 7.37 (m, 4H).
9-[(E)-2-(4-methylphenyl)ethenyl]phenanthrene, FEN-CH$_3$	
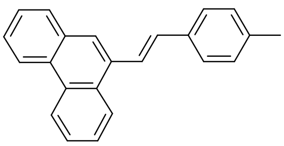	Synthesized from 9-bromophenanthrene (257 mg, 1.00 mmol) and 4-methylstyrene (0.142 mg, 1.20 mmol) in 87% yield. **^{1}H NMR (400 MHz, DMSO) δ [ppm]:** 8.94 – 8.89 (m, 1H), 8.85 – 8.80 (m, 1H), 8.49 – 8.42 (m, 1H), 8.18 (s, 1H), 8.08 – 8.00 (m, 2H), 7.79 – 7.64 (m, 6H), 7.36 (d, *J* = 16.0 Hz, 1H), 7.30 – 7.24 (m, 2H), 2.37 (s, 3H).
9-[(E)-2-(4-methoxyphenyl)ethenyl]phenanthrene[9], FEN-OCH$_3$	
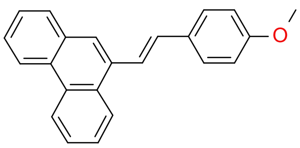	Synthesized from 9-bromophenanthrene (257 mg, 1.00 mmol) and 4-methoxystyrene (0.161 mg, 1.20 mmol) in 96% yield. **^{1}H NMR (400 MHz, DMSO) δ [ppm]:** 8.93 – 8.87 (m, 1H), 8.85 – 8.80 (m, 1H), 8.49 – 8.43 (m, 1H), 8.16 (s, 1H), 8.08 – 8.01 (m, 1H), 7.94 (d, *J* = 16.0 Hz, 1H), 7.79 – 7.72 (m, 4H), 7.71 – 7.63 (m, 2H), 7.34 (d, *J* = 16.0 Hz, 1H), 7.05 – 6.98 (m, 2H), 3.82 (s, 3H).

9-[(E)-2-(2-pyridyl)ethenyl]phenantrene, FEN-PYR	
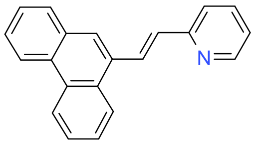	Synthesized from 9-bromophenanthrene (257 mg, 1.00 mmol) and 2-vinylpyridine (0.158 mg, 1.20 mmol) in 92% yield. **^{1}H NMR (400 MHz, DMSO) δ [ppm]:** 8.95 – 8.90 (m, 1H), 8.87 – 8.82 (m, 1H), 8.70 – 8.65 (m, 1H), 8.52 (d, *J* = 15.8 Hz, 1H), 8.40 – 8.35 (m, 1H), 8.28 (s, 1H), 8.11 – 8.06 (m, 1H), 7.90 – 7.83 (m, 1H), 7.81 – 7.74 (m, 3H), 7.74 – 7.66 (m, 2H), 7.48 (d, *J* = 15.7 Hz, 1H), 7.34 (ddd, *J* = 7.5, 4.8, 1.2 Hz, 1H).
9-[(E)-2-(4-chlorophenyl)ethenyl]phenanthrene, FEN-Cl	
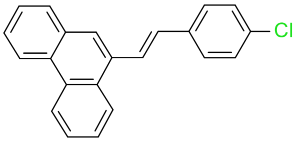	Synthesized from 9-bromophenanthrene (257 mg, 1.00 mmol) and 4-chlorostyrene (0.167 mg, 1.20 mmol) in 65% yield. **^{1}H NMR (400 MHz, DMSO) δ [ppm]:** 8.95 – 8.89 (m, 1H), 8.88 – 8.81 (m, 1H), 8.49 – 8.44 (m, 1H), 8.21 (s, 1H), 8.14 (d, *J* = 16.1 Hz, 1H), 8.10 – 8.03 (m, 1H), 7.90 – 7.82 (m, 2H), 7.81 – 7.64 (m, 4H), 7.54 – 7.47 (m, 2H), 7.40 (d, *J* = 16.0 Hz, 1H).
9-[(E)-2-(4-fluorophenyl)ethenyl]phenanthrene, FEN-F	
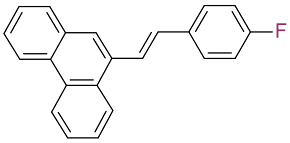	Synthesized from 9-bromophenanthrene (257 mg, 1.00 mmol) and 4-fluorostyrene (0.146 mg, 1.20 mmol) in 45% yield. **^{1}H NMR (400 MHz, DMSO) δ [ppm]:** ^{1}H NMR (400 MHz, DMSO) δ 8.94 – 8.90 (m, 1H), 8.87 – 8.82 (m, 1H), 8.50 – 8.44 (m, 1H), 8.19 (s, 1H), 8.11 – 8.04 (m, 3H), 7.92 – 7.85 (m, 2H), 7.83 – 7.67 (m, 5H), 7.40 (d, *J* = 16.1 Hz, 1H).

NMR spectra of the synthesized compounds

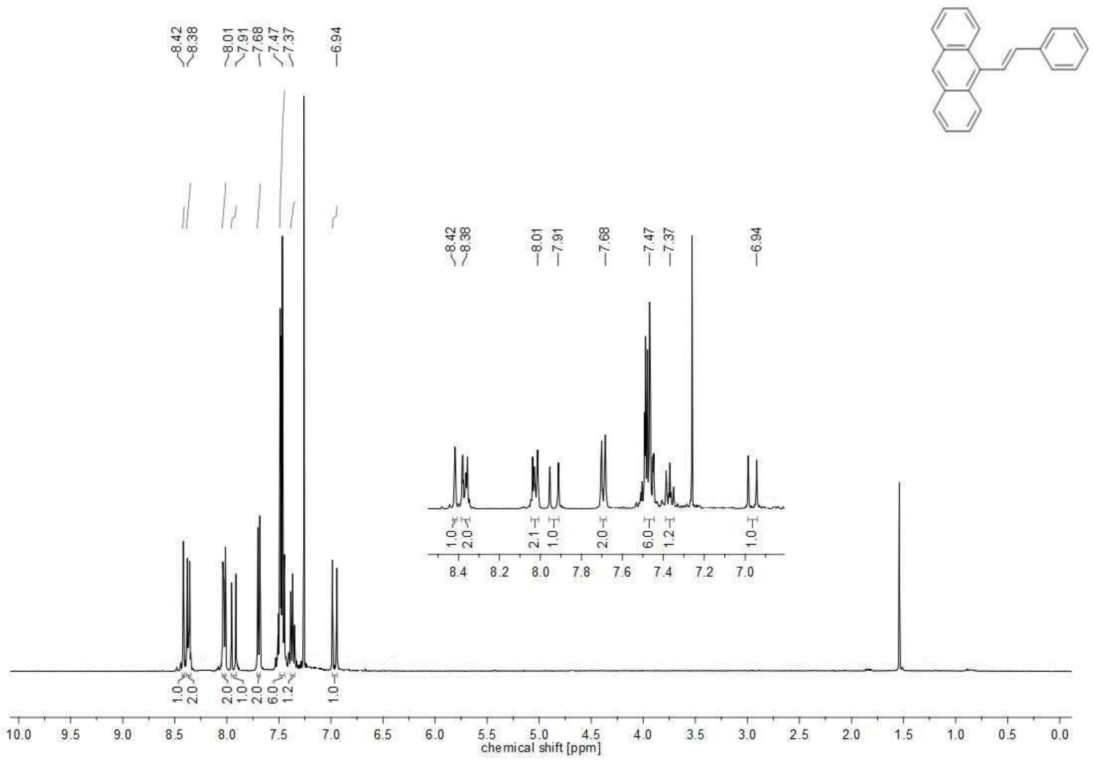

Figure S.1. ^{1}H NMR spectrum of 9-[(E)-2-phenylethenyl]anthracene, ANT-H

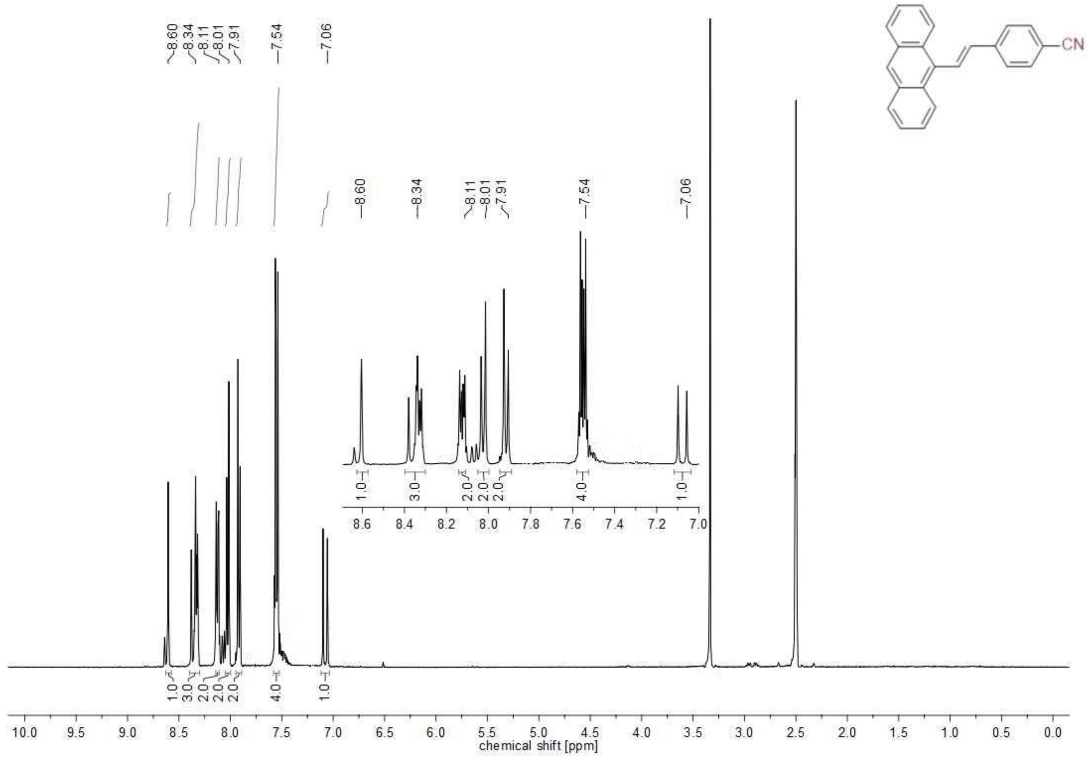

Figure S.2. ^{1}H NMR spectrum of 9-[(E)-2-(4-cyanophenyl)ethenyl]anthracene, ANT-CN

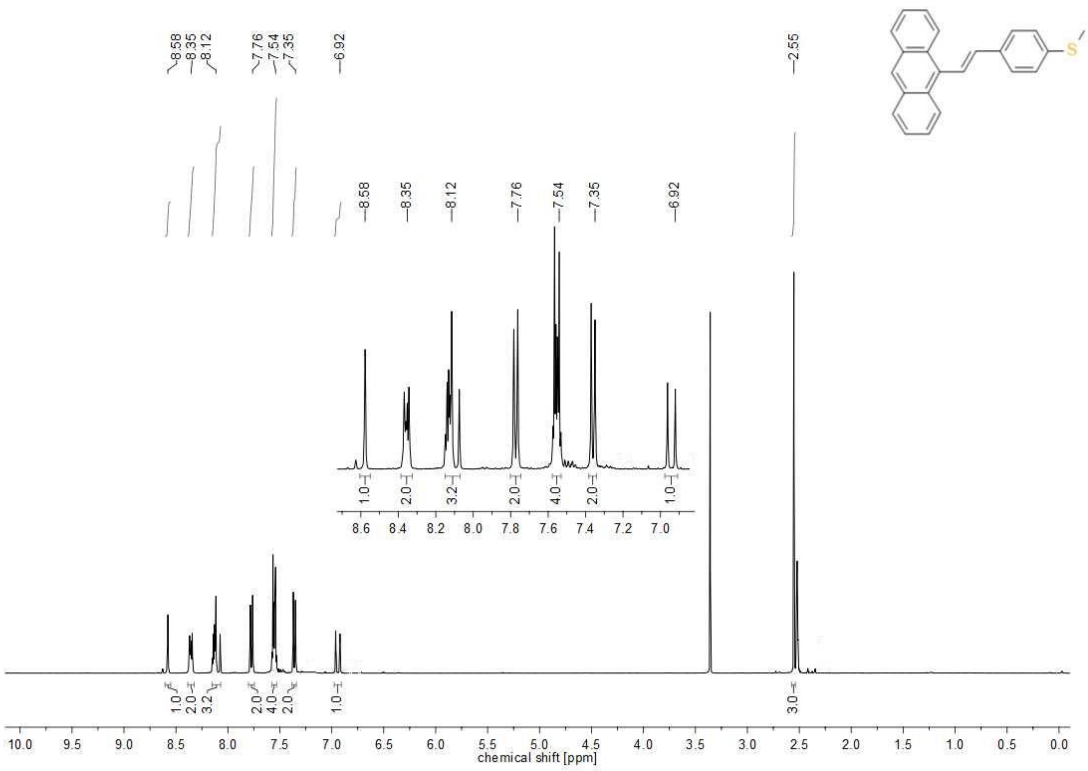

Figure S.3. ^{1}H NMR spectrum of 9-[(E)-2-[4-(methylsulfanyl)phenyl]ethenyl]anthracene, **ANT-SCH_3**

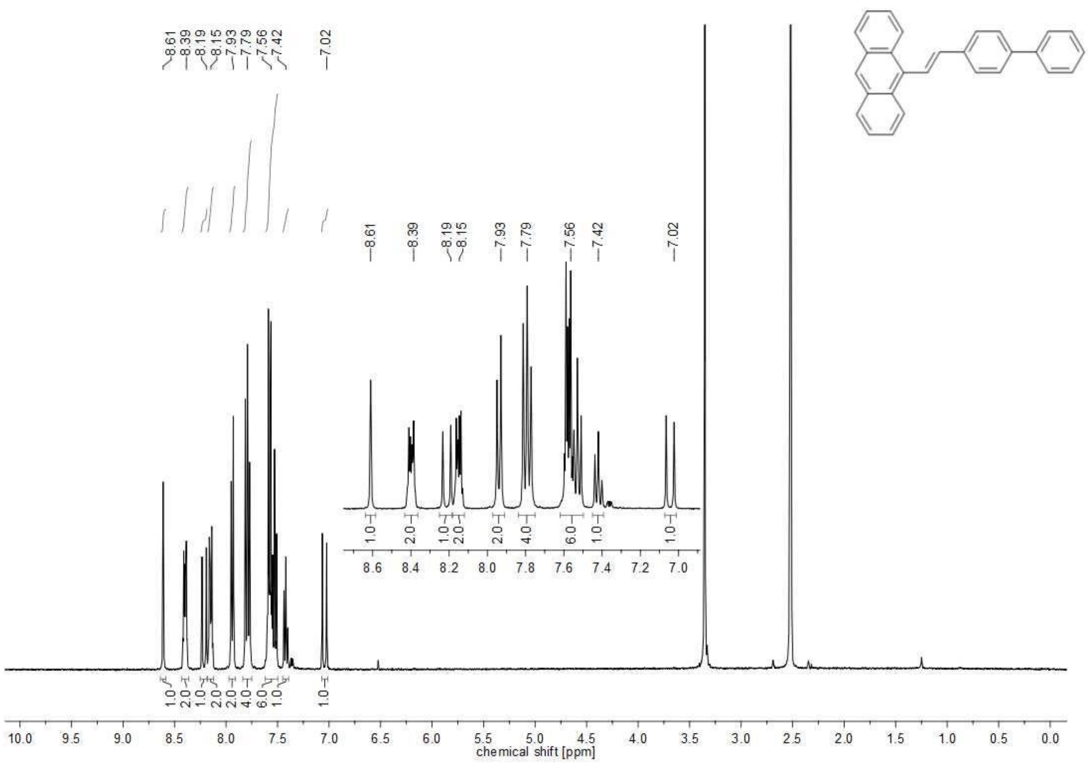

Figure S.4. ^{1}H NMR spectrum of 9-[(E)-2-([1,1'-biphenyl]-4-yl)ethenyl]anthracene, **ANT-C_6H_5**

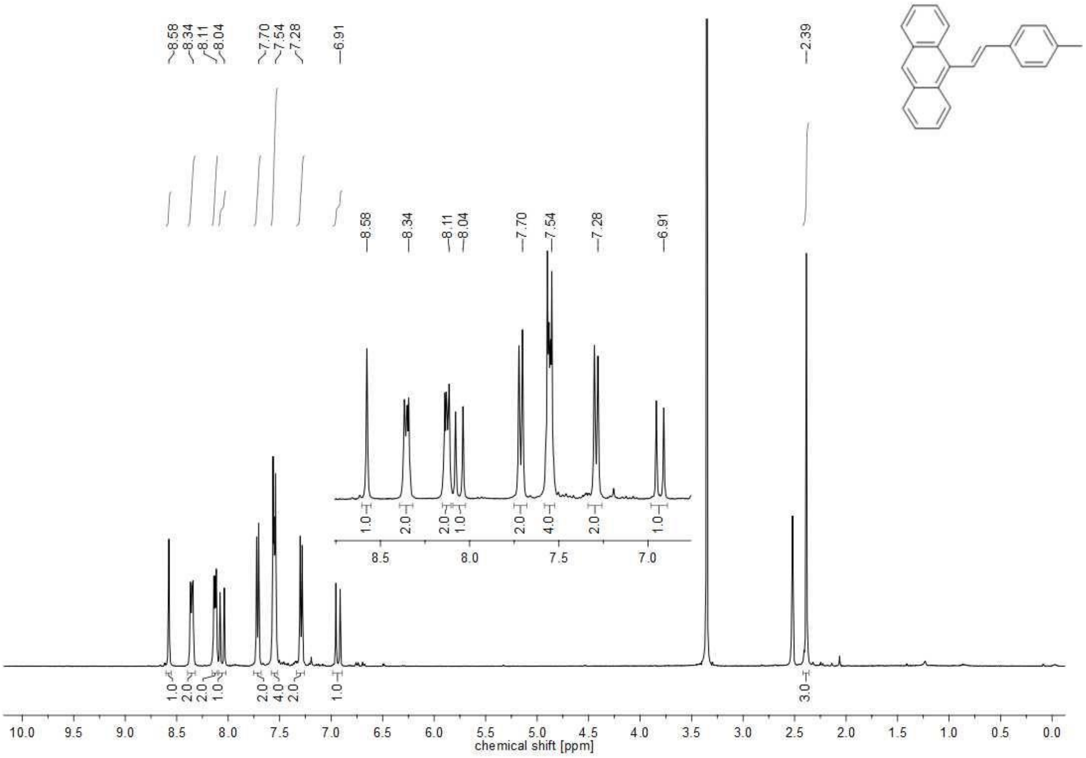

Figure S.5. ^{1}H NMR spectrum of 9-[(E)-2-(4-methylphenyl)ethenyl]anthracene, **ANT-CH$_3$**

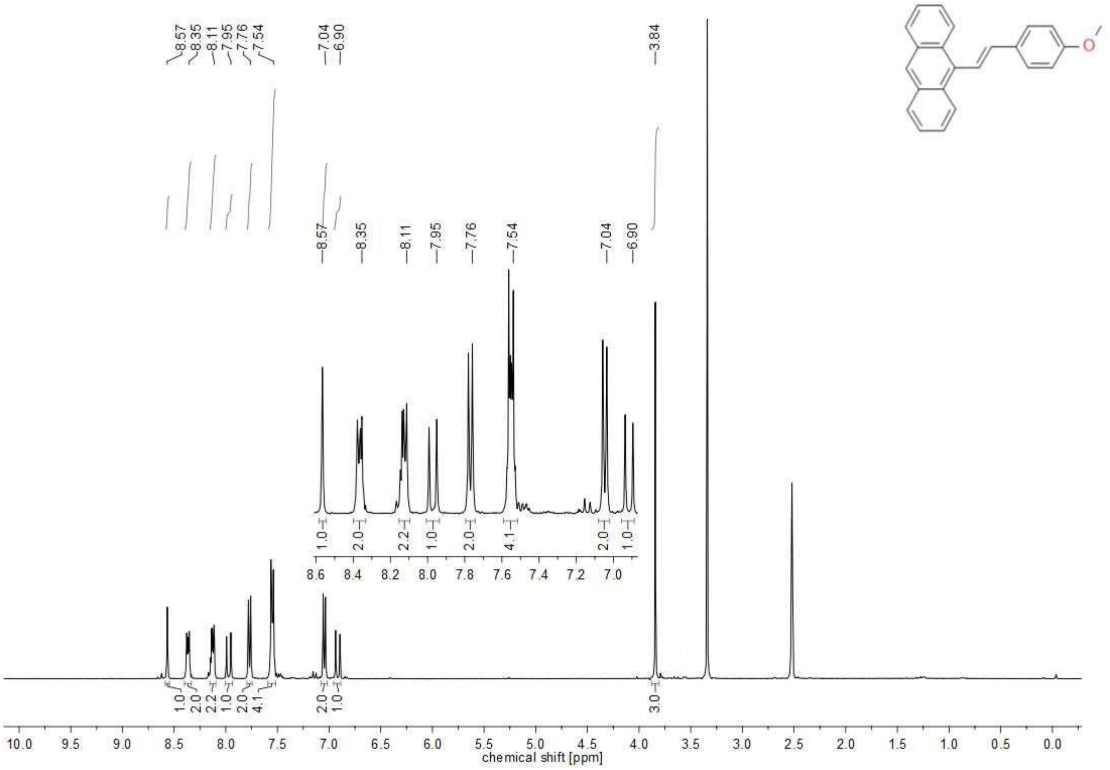

Figure S.6. ^{1}H NMR spectrum of 9-[(E)-2-(4-methoxyphenyl)ethenyl]anthracene, **ANT-OCH$_3$**

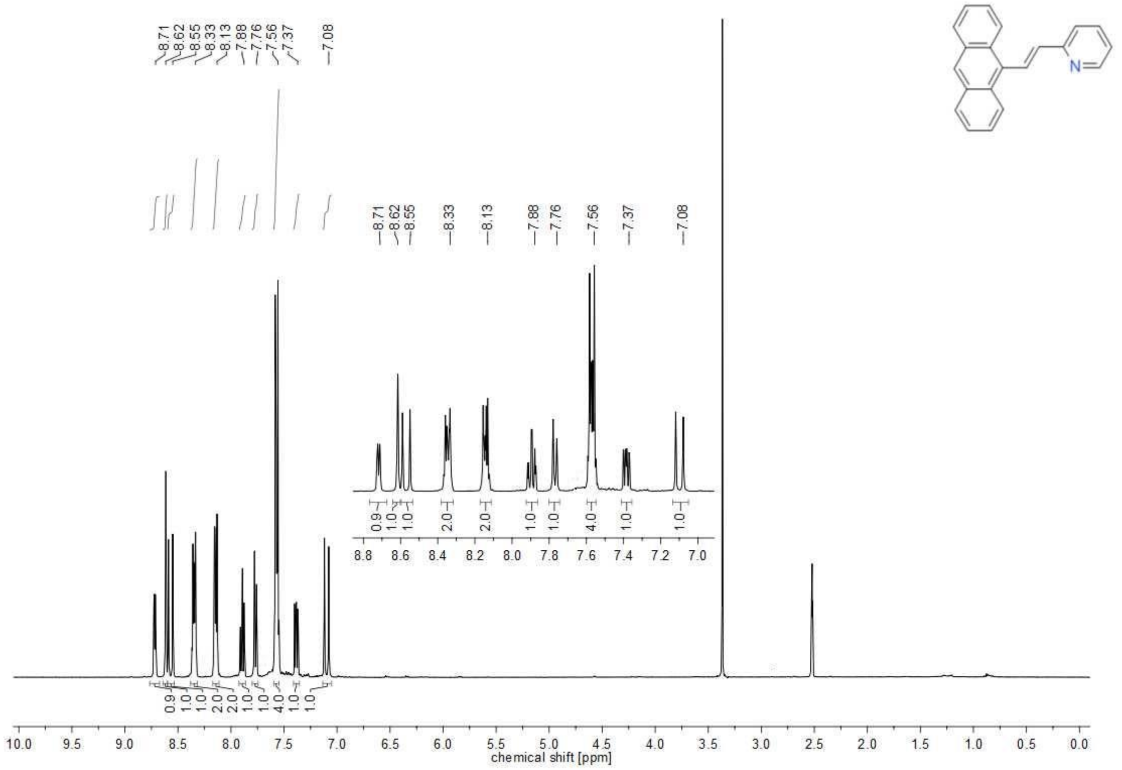

Figure S.7. ^{1}H NMR spectrum of *9-[(E)-2-(2-pyridyl)ethenyl]anthracene,* ANT-PYR

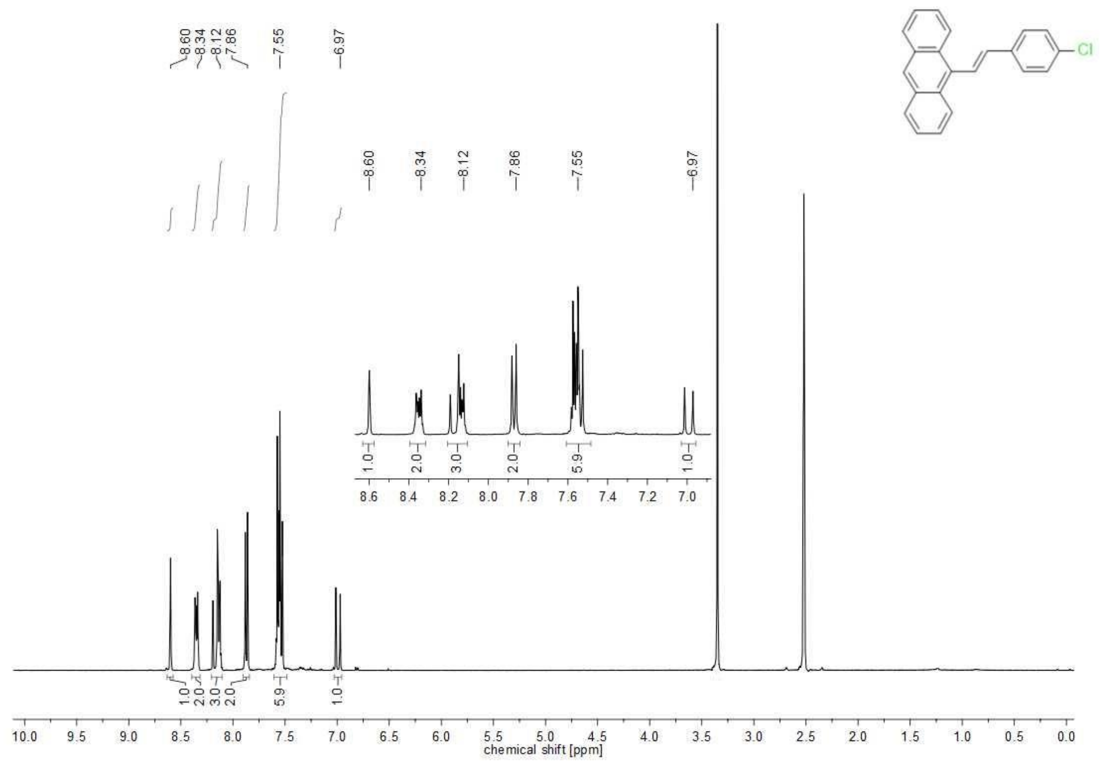

Figure S.8. ^{1}H NMR spectrum of *9-[(E)-2-(4-chlorophenyl)ethenyl]anthracene,* ANT-Cl

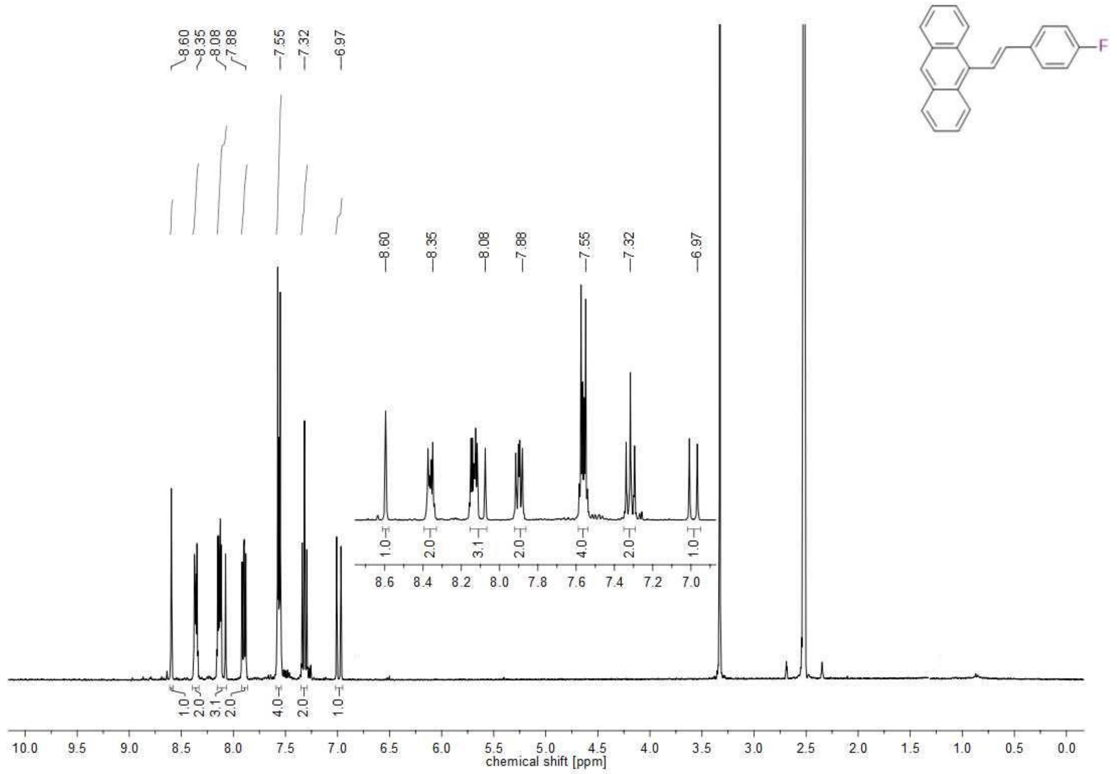

Figure S.9. ^{1}H NMR spectrum of *9-[(E)-2-(4-fluorophenyl)ethenyl]anthracene,* ANT-F

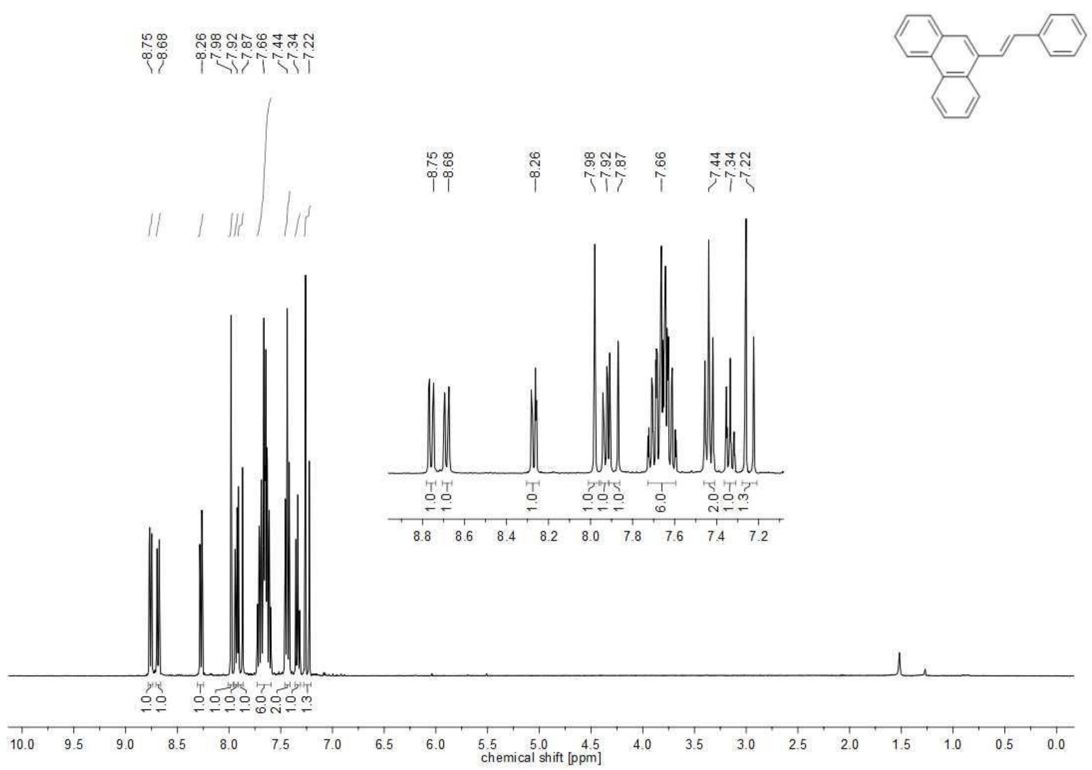

Figure S.10. ^{1}H NMR spectrum of *9-[(E)-2-phenylethenyl] phenanthrene,* FEN-H

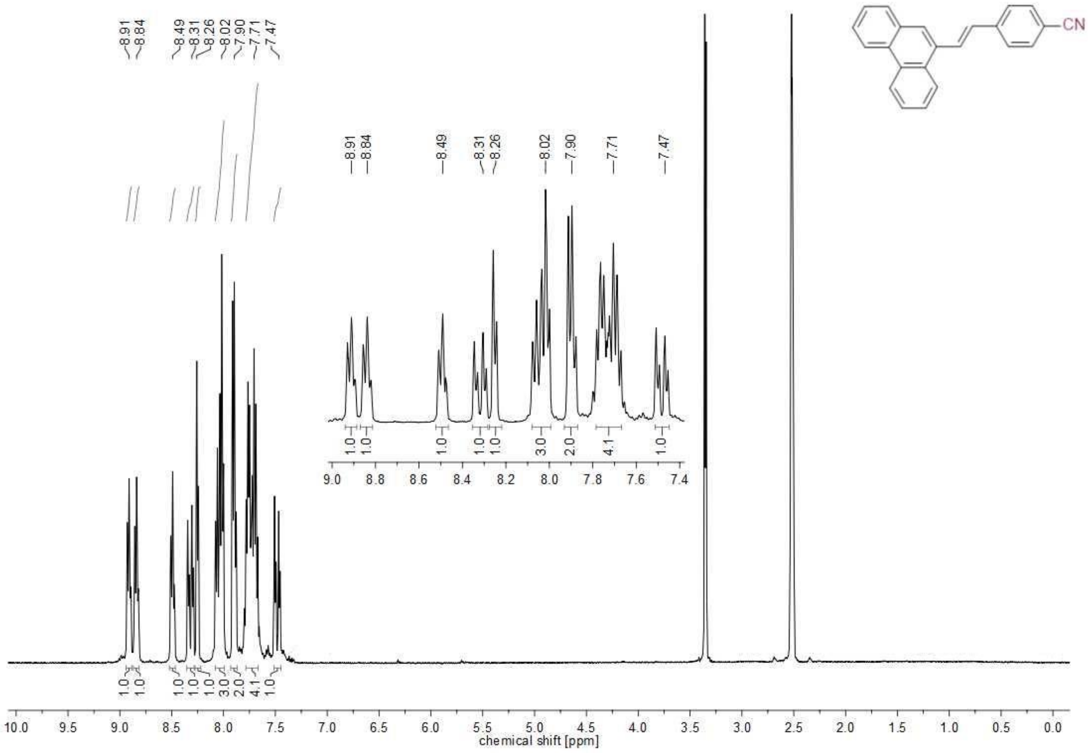

Figure S.11. ¹H NMR spectrum of *9-[(E)-2-(4-cyanophenyl)ethenyl]phenanthrene,* FEN-CN

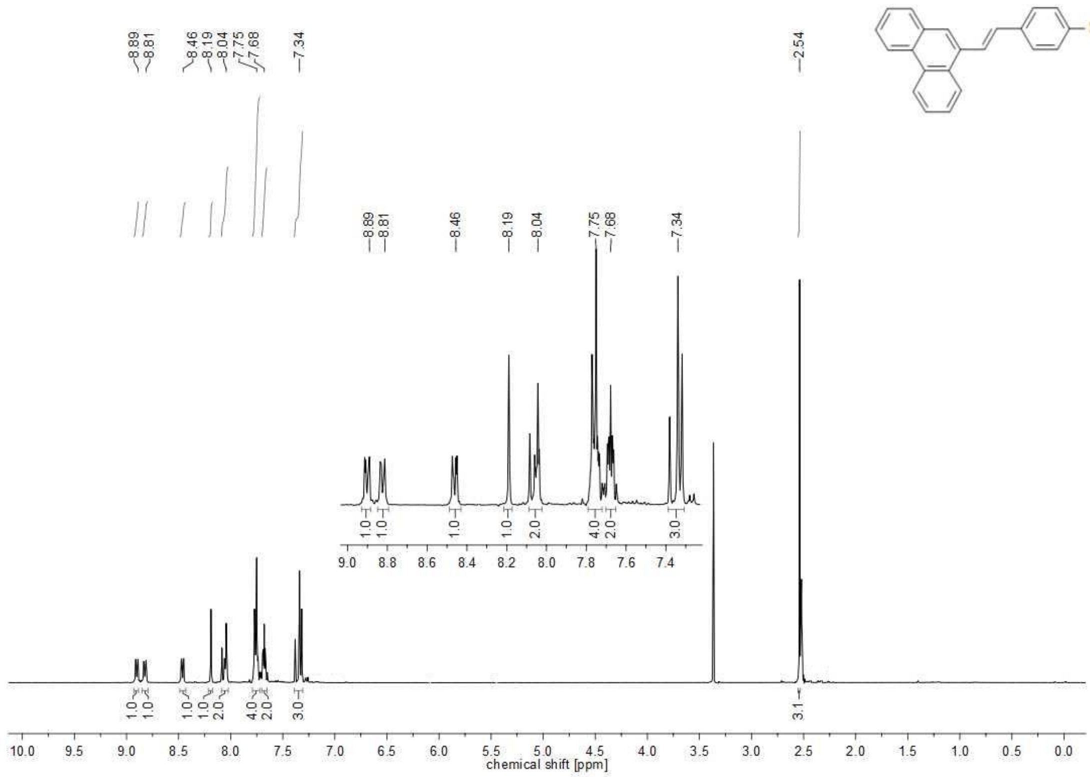

Figure S.12. ¹H NMR spectrum of *9-[(E)-2-[4-(methylsulfanyl)phenyl]ethenyl]phenanthrene,* FEN-SCH_3

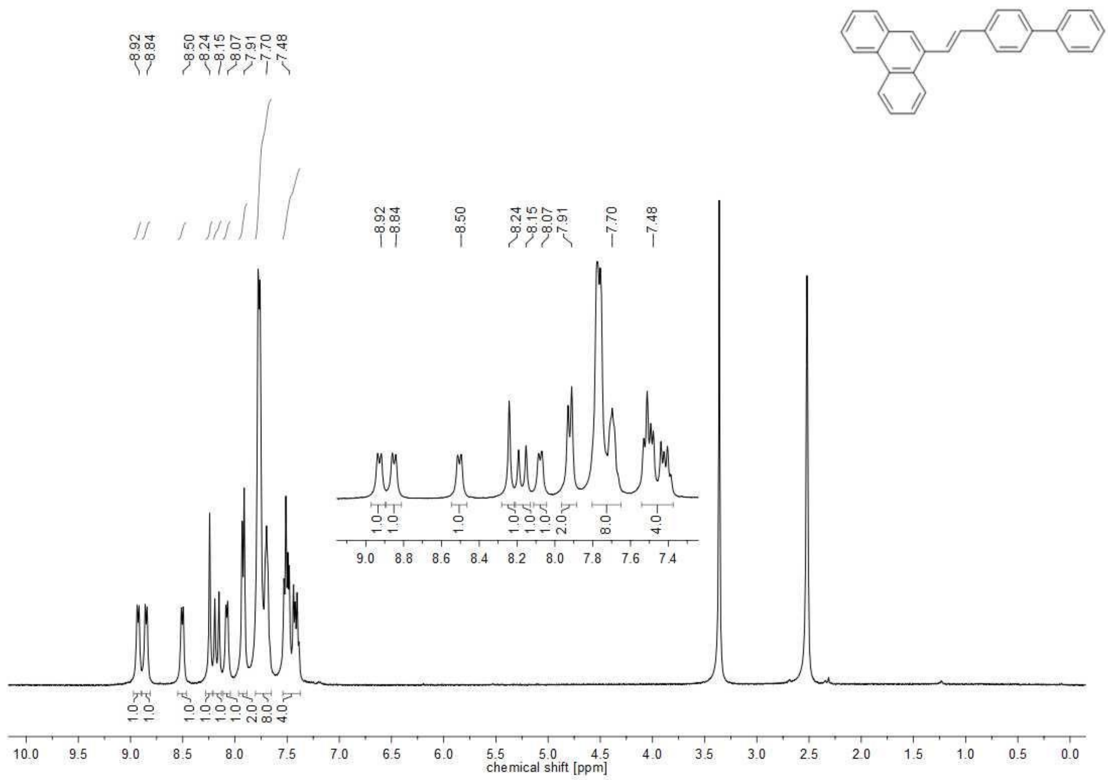

Figure S.13. [1]H NMR spectrum of *9-[(E)-2-([1,1'-biphenyl]-4-yl)ethenyl]phenanthrene,* FEN-C_6H_5

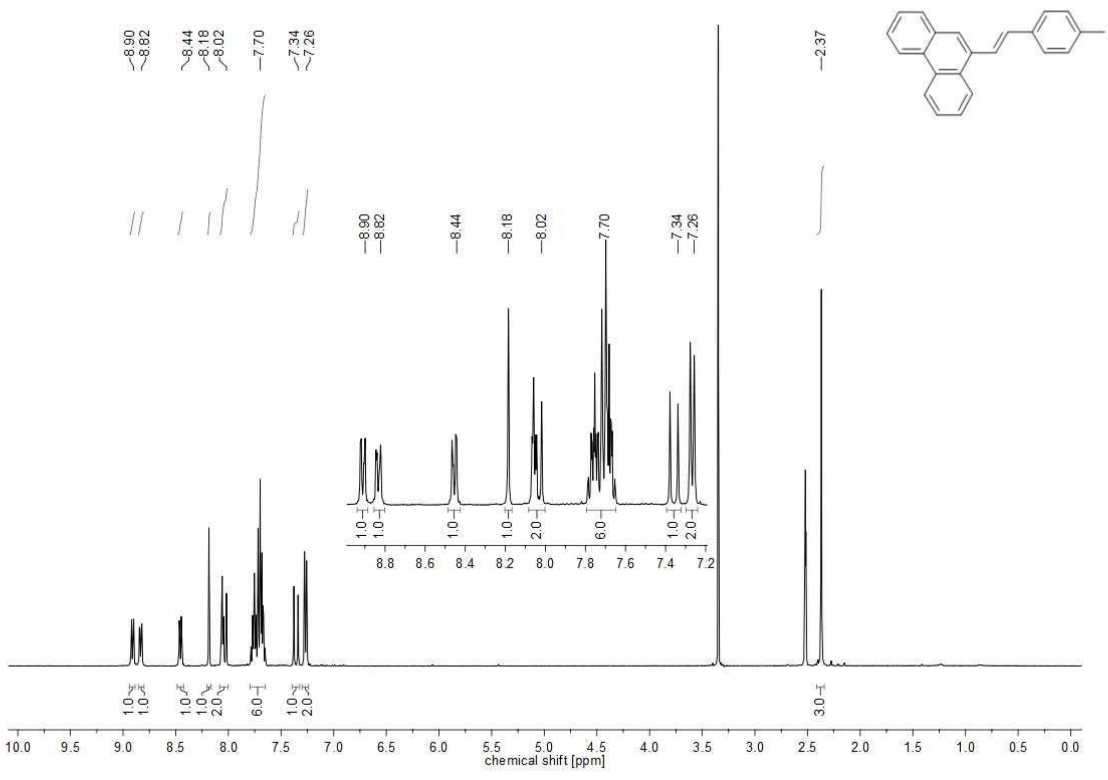

Figure S.14. [1]H NMR spectrum of *9-[(E)-2-(4-methylphenyl)ethenyl]phenanthrene,* FEN-CH_3

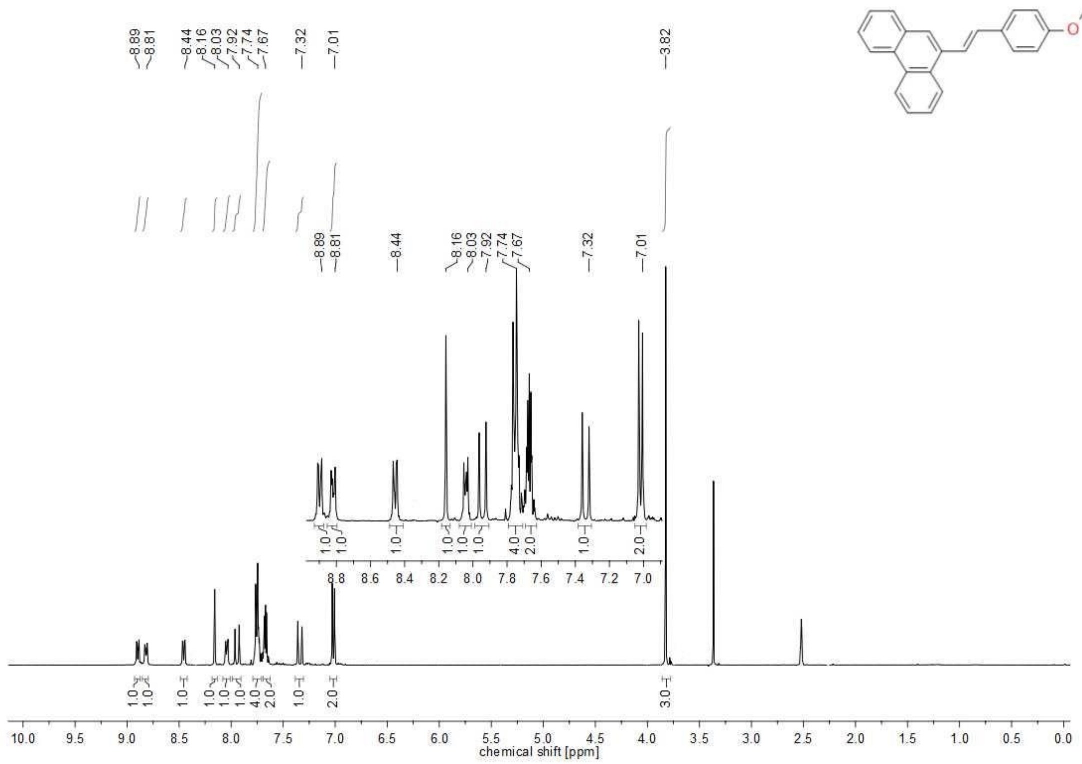

Figure S.15. [1]H NMR spectrum of *9-[(E)-2-(4-methoxyphenyl)ethenyl]phenanthrene,* FEN-OCH_3

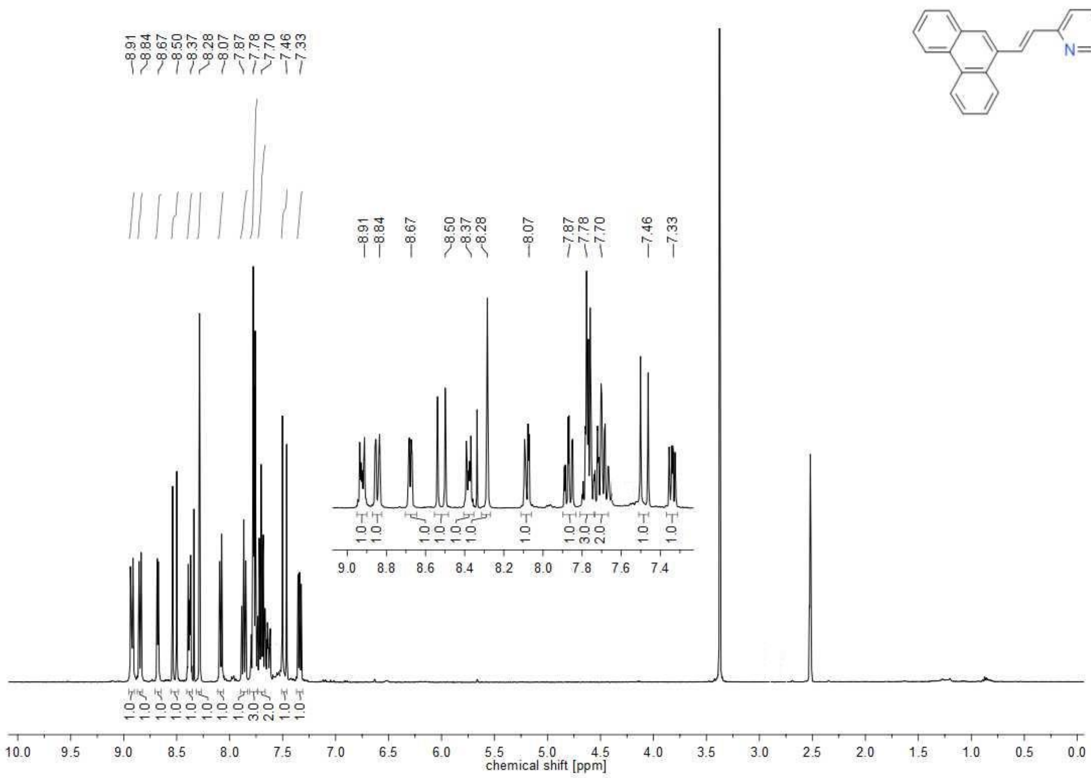

Figure S.16. [1]H NMR spectrum of *9-[(E)-2-(2-pyridyl)ethenyl]phenanthrene,* FEN-PYR

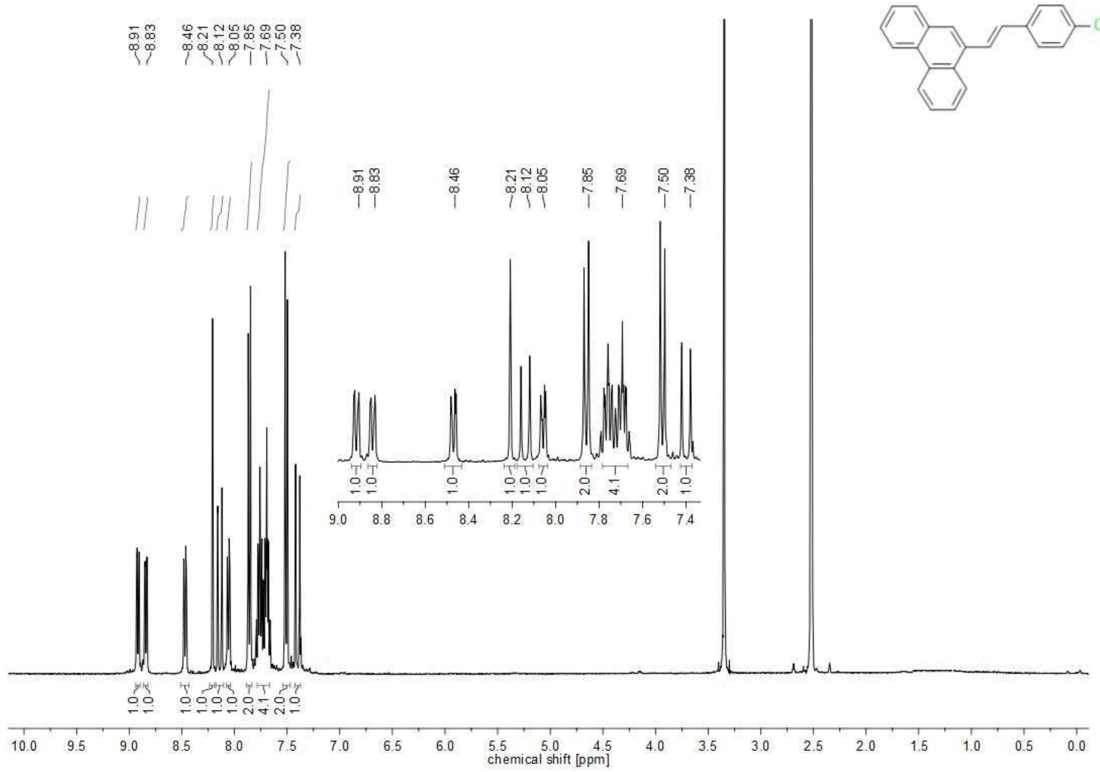

Figure S.17. [1]H NMR spectrum of *9-[(E)-2-(4-chlorophenyl)ethenyl]phenanthrene,* FEN-Cl

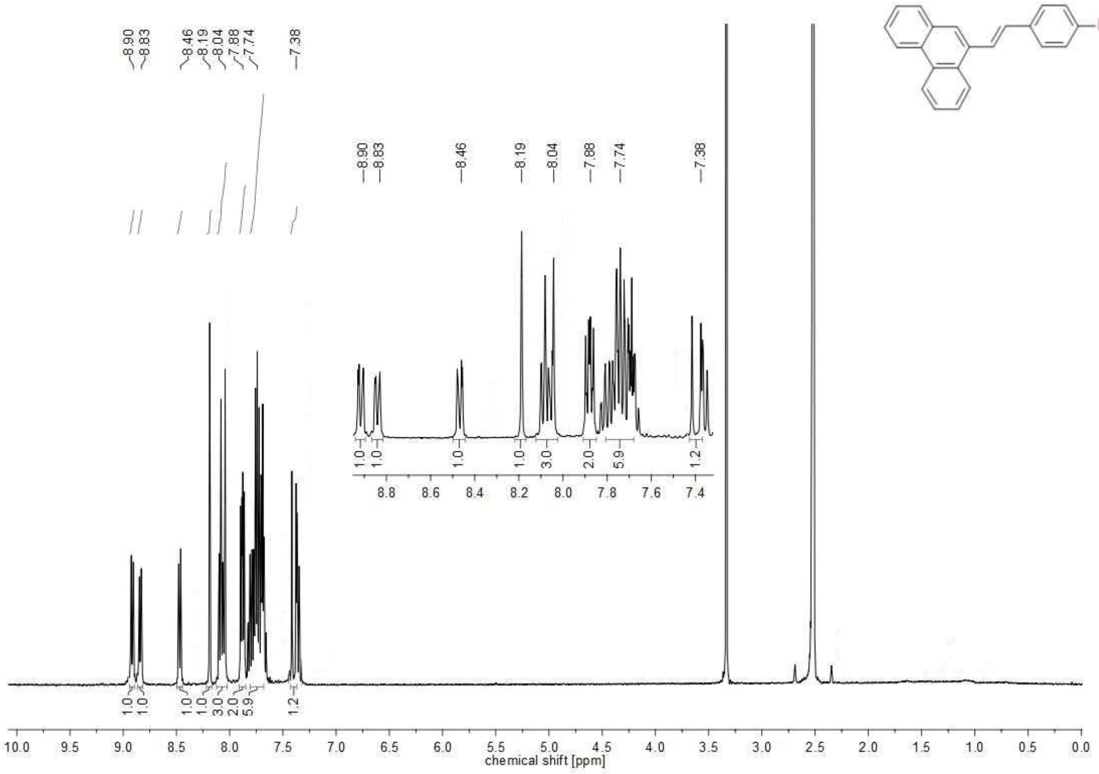

Figure S.18. [1]H NMR spectrum of *9-[(E)-2-(4-fluorophenyl)ethenyl]phenanthrene,* FEN-F

Structures of used commercial compounds

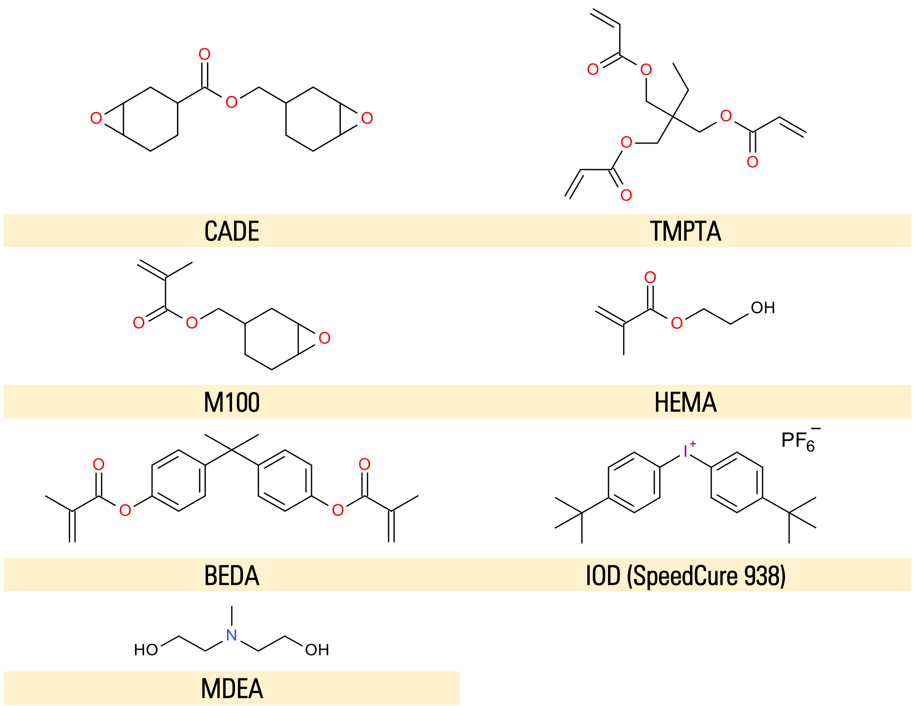

Figure S.19. Structures of used commercial compounds.

Cyclic voltammetry for oxidation and reduction processes in acetonitrile

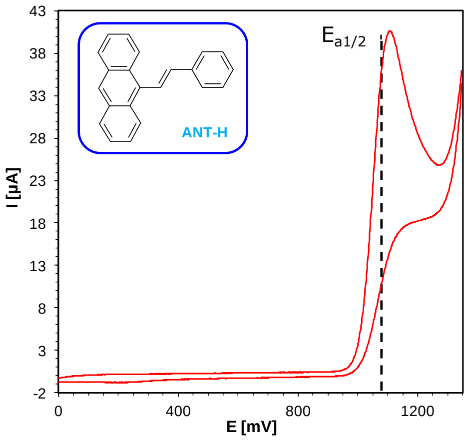

Figure S.20. Cyclic voltammetry of the oxidation process for the compound **ANT-H** in acetonitrile.

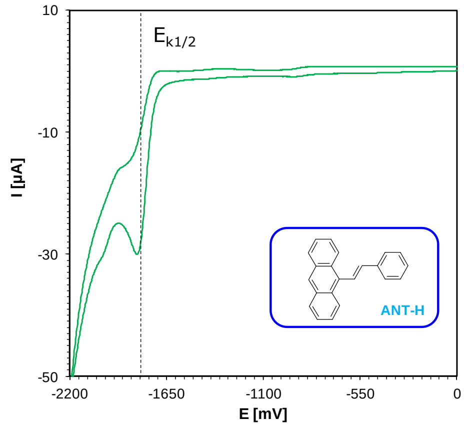

Figure S.21. Cyclic voltammetry of the reduction process for the compound **ANT-H** in acetonitrile.

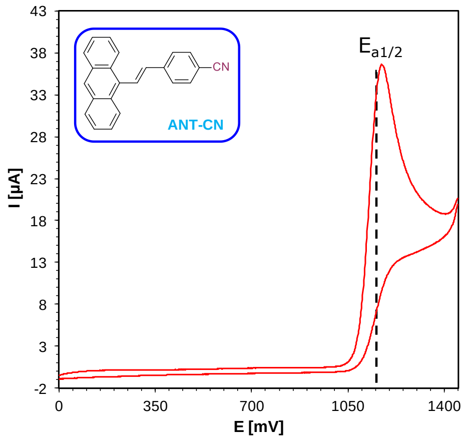

Figure S.22. Cyclic voltammetry of the oxidation process for the compound **ANT-CN** in acetonitrile.

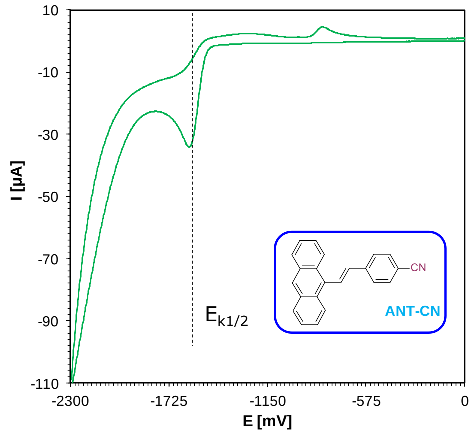

Figure S.23. Cyclic voltammetry of the reduction process for the compound **ANT-CN** in acetonitrile.

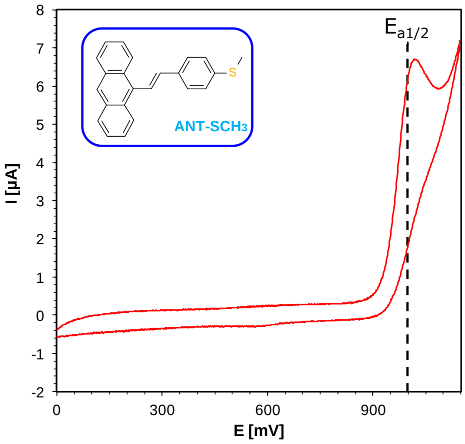

Figure S.24. Cyclic voltammetry of the oxidation process for thecompound **ANT-SCH$_3$** in acetonitrile.

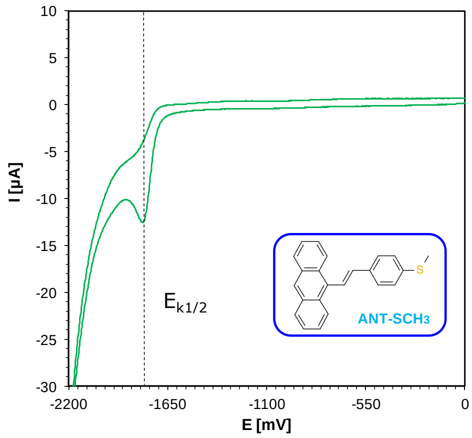

Figure S.25. Cyclic voltammetry of the reduction process for the compound **ANT- SCH$_3$** in acetonitrile.

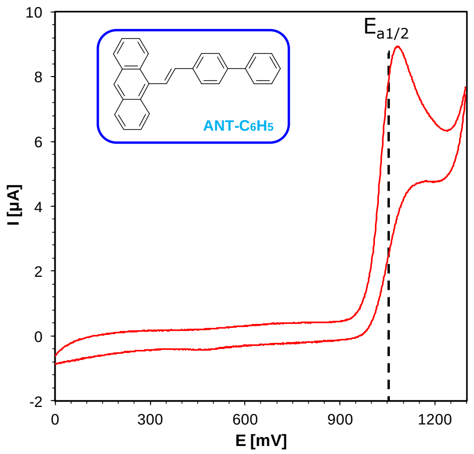

Figure S.26. Cyclic voltammetry of the oxidation process for the compound ANT-C_6H_5 in acetonitrile.

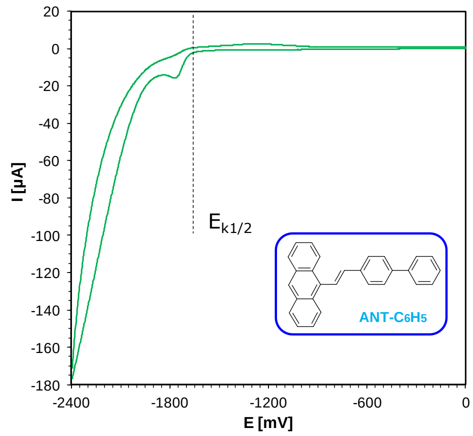

Figure S.27. Cyclic voltammetry of the reduction process for the compound ANT- C_6H_5 in acetonitrile.

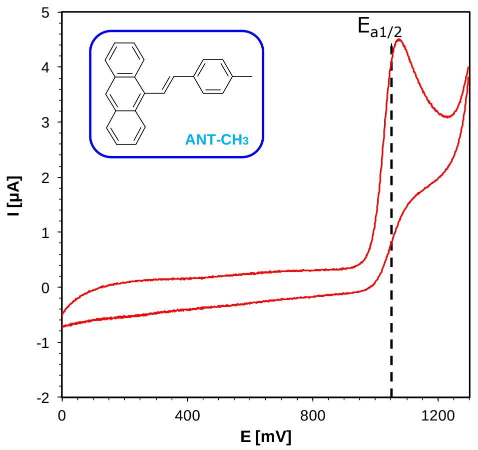

Figure S.28. Cyclic voltammetry of the oxidation process for the compound ANT-CH_3 in acetonitrile.

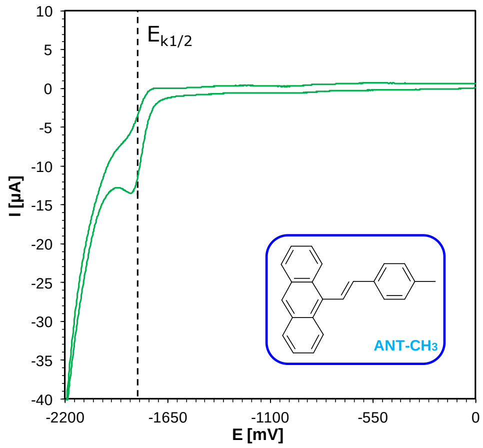

Figure S.29. Cyclic voltammetry of the reduction process for the compound ANT- CH_3 in acetonitrile.

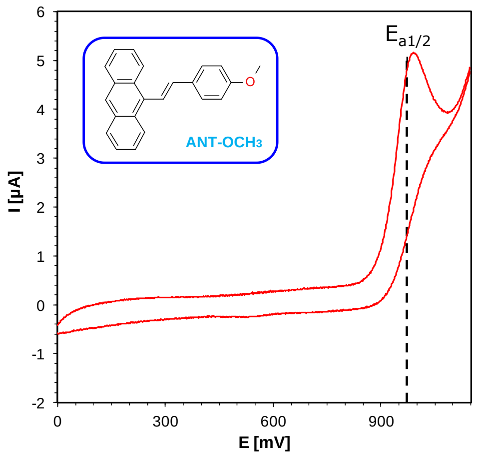

Figure S.30. Cyclic voltammetry of the oxidation process for the compound ANT-OCH_3 in acetonitrile.

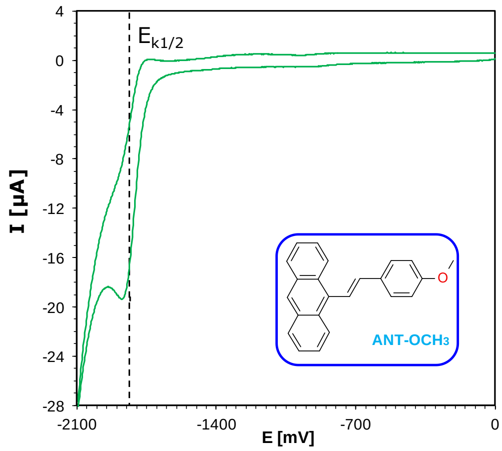

Figure S.31. Cyclic voltammetry of the reduction process for the compound ANT- OCH_3 in acetonitrile.

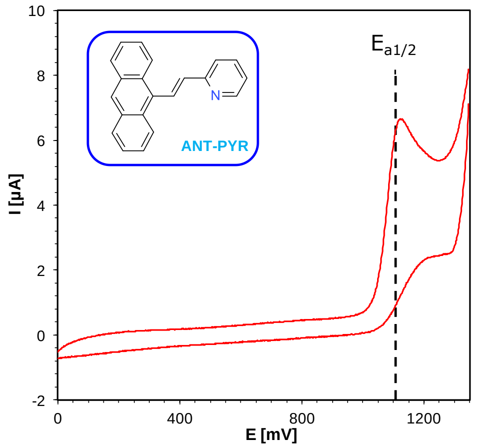

Figure S.32. Cyclic voltammetry of the oxidation process for the compound **ANT-PYR** in acetonitrile.

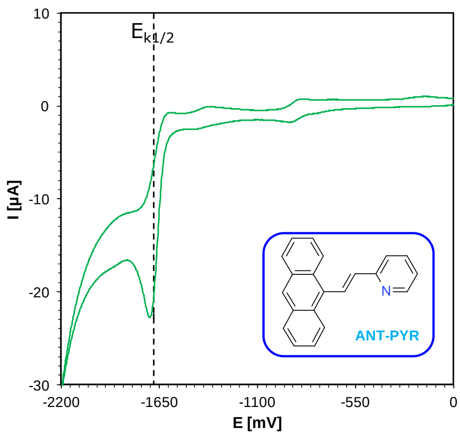

Figure S.33. Cyclic voltammetry of the reduction process for the compound **ANT- PYR** in acetonitrile.

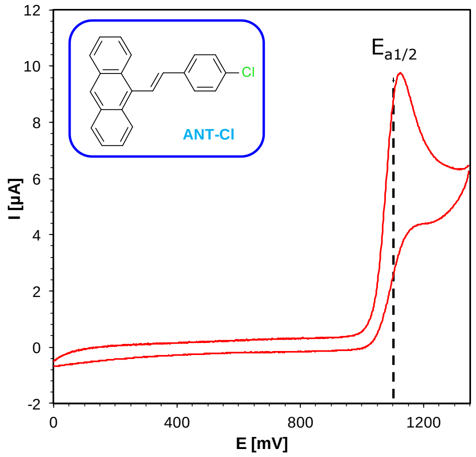

Figure S.34. Cyclic voltammetry of the oxidation process for the compound **ANT-Cl** in acetonitrile.

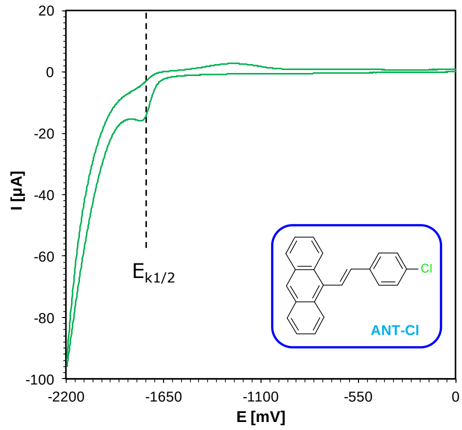

Figure S.35. Cyclic voltammetry of the reduction process for the compound **ANT-Cl** in acetonitrile.

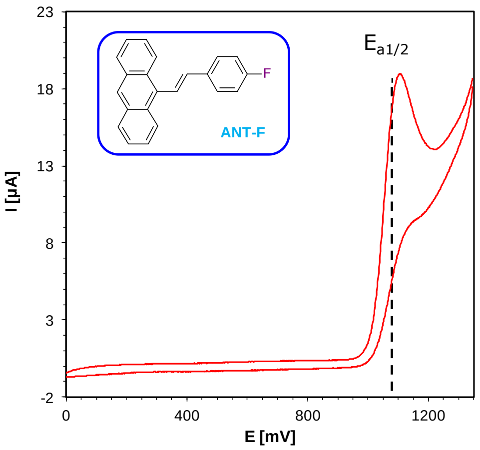

Figure S.36. Cyclic voltammetry of the oxidation process for the compound **ANT-F** in acetonitrile.

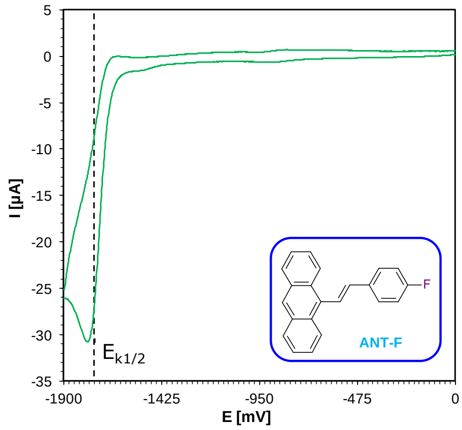

Figure S.37. Cyclic voltammetry of the reduction process for the compound **ANT-F** in acetonitrile.

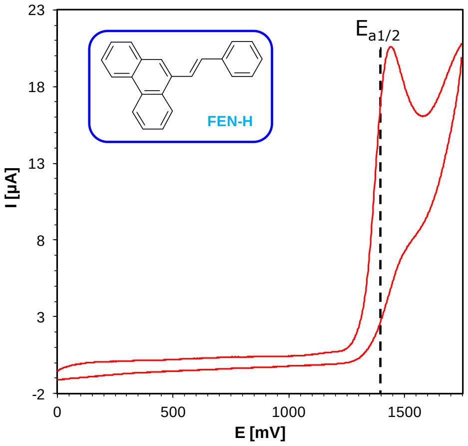

Figure S.38. Cyclic voltammetry of the oxidation process for the compound **FEN-H** in acetonitrile.

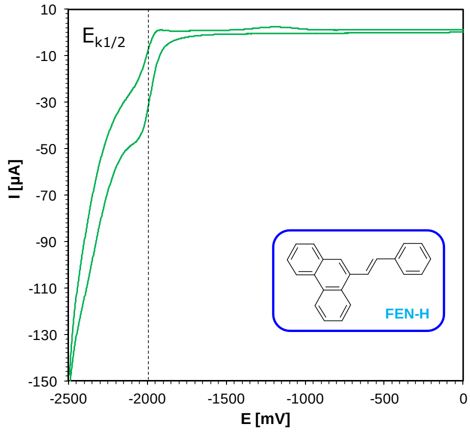

Figure S.39. Cyclic voltammetry of the reduction process for the compound **FEN-H** in acetonitrile.

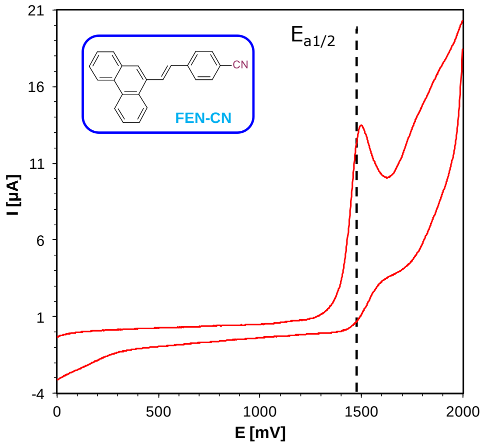

Figure S.40. Cyclic voltammetry of the oxidation process for the compound **FEN-CN** in acetonitrile.

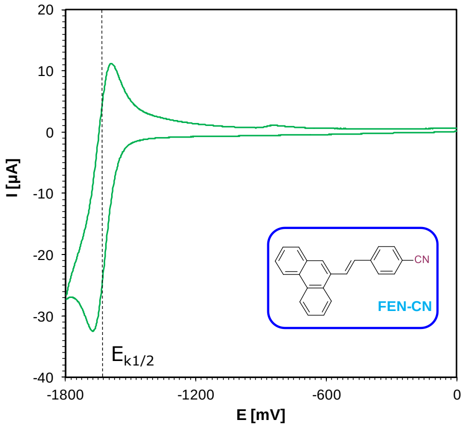

Figure S.41. Cyclic voltammetry of the reduction process for the compound **FEN-CN** in acetonitrile.

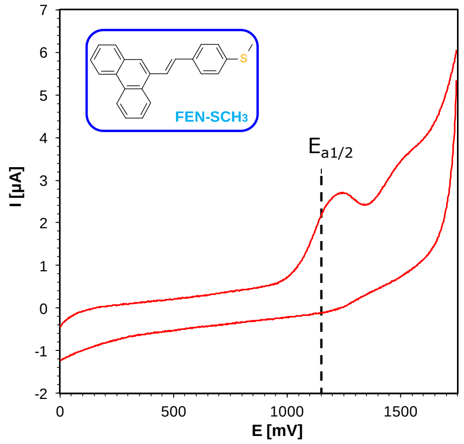

Figure S.42. Cyclic voltammetry of the oxidation process for the compound **FEN-SCH$_3$** in acetonitrile.

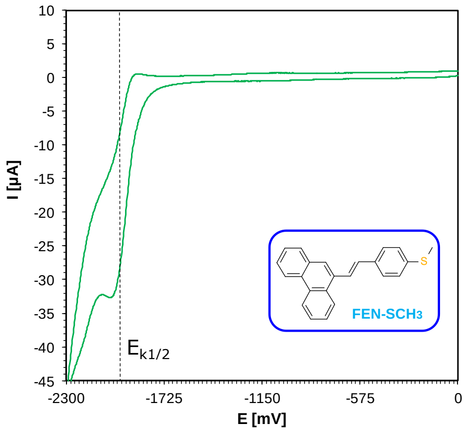

Figure S.43. Cyclic voltammetry of the reduction process for the compound **FEN-SCH$_3$** in acetonitrile.

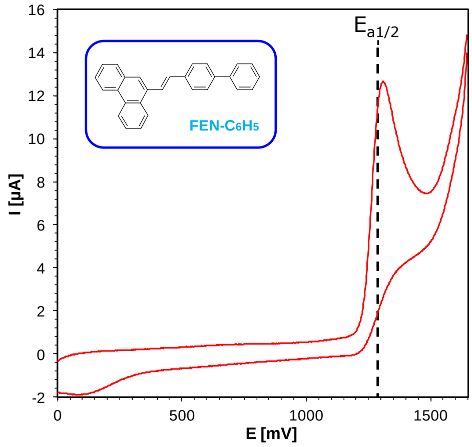

Figure S.44. Cyclic voltammetry of the oxidation process for the compound **FEN-C_6H_5** in acetonitrile.

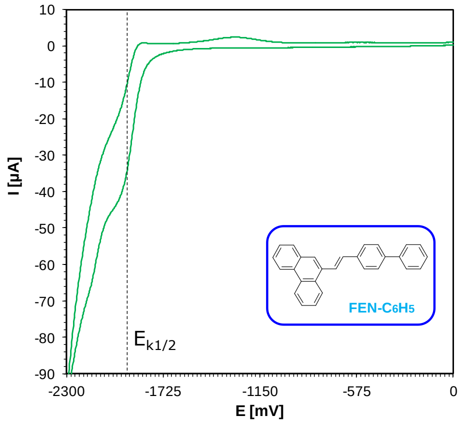

Figure S.45. Cyclic voltammetry of the reduction process for the compound **FEN-C_6H_5** in acetonitrile.

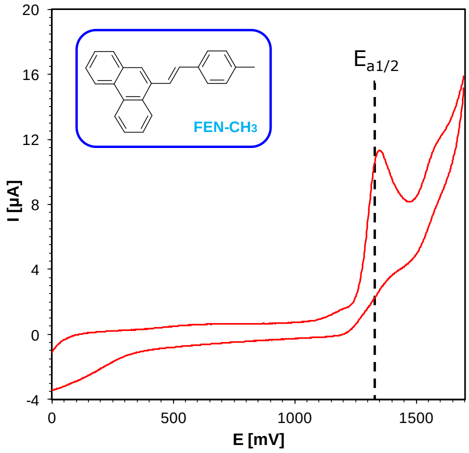

Figure S.46. Cyclic voltammetry of the oxidation process for the compound **FEN-CH_3** in acetonitrile.

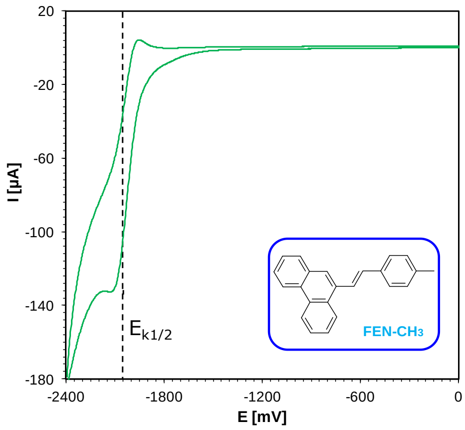

Figure S.47. Cyclic voltammetry of the reduction process for the compound **FEN-CH_3** in acetonitrile.

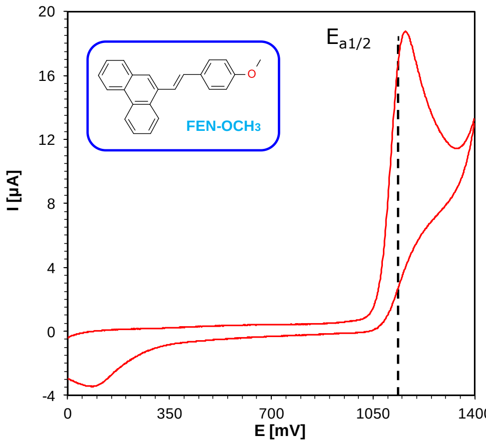

Figure S.48. Cyclic voltammetry of the oxidation process for the compound **FEN-OCH_3** in acetonitrile.

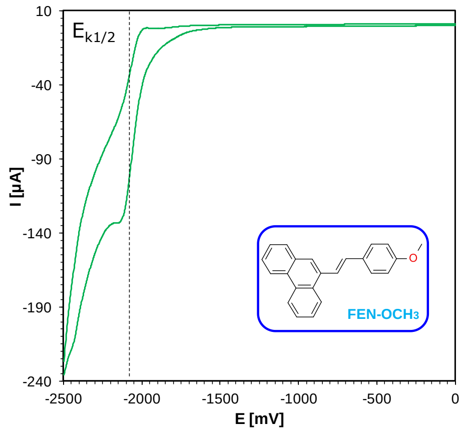

Figure S.49. Cyclic voltammetry of the reduction process for the compound **FEN-OCH_3** in acetonitrile.

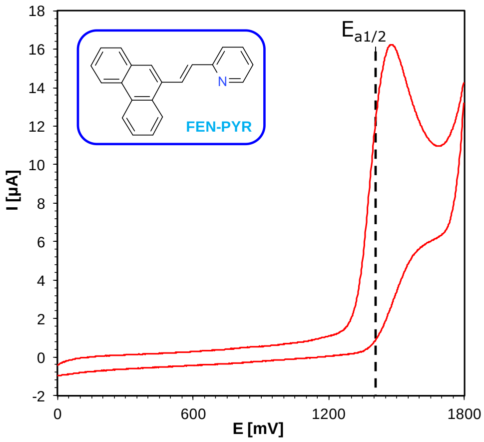

Figure S.50. Cyclic voltammetry of the oxidation process for the compound FEN-PYR in acetonitrile.

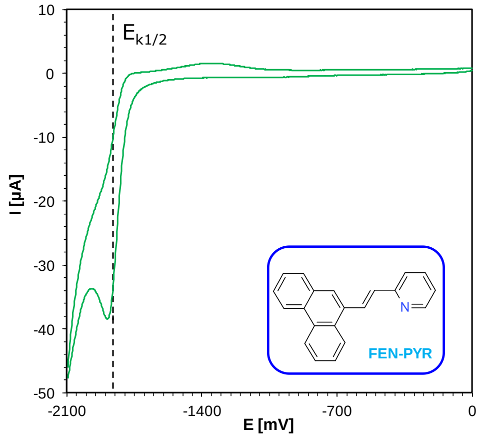

Figure S.51. Cyclic voltammetry of the reduction process for the compound FEN-PYR in acetonitrile.

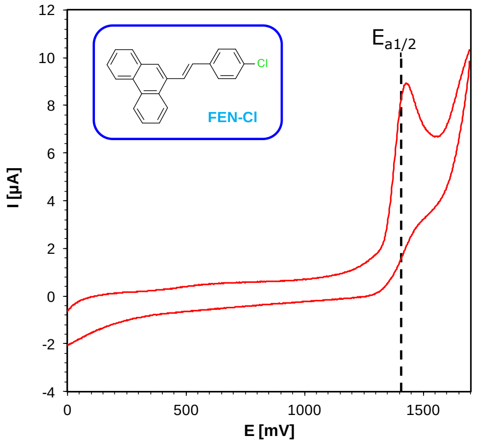

Figure S.52. Cyclic voltammetry of the oxidation process for the compound FEN-Cl in acetonitrile.

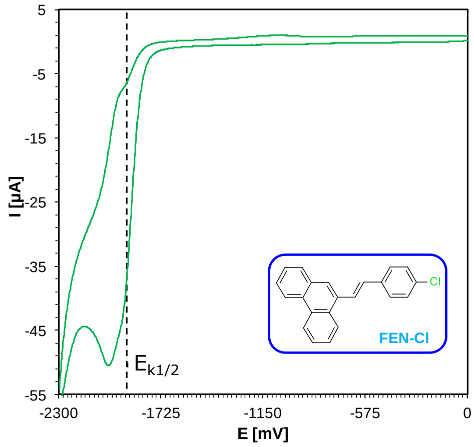

Figure S.53. Cyclic voltammetry of the reduction process for the compound FEN-Cl in acetonitrile.

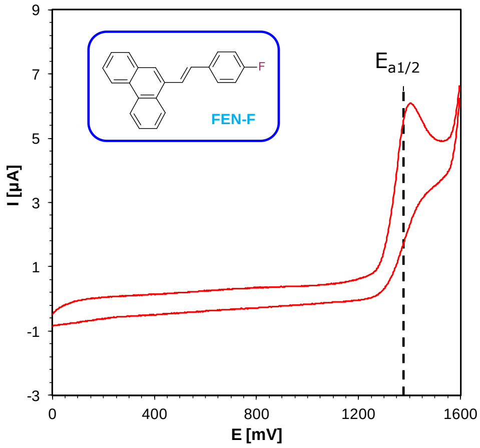

Figure S.54. Cyclic voltammetry of the oxidation process for the compound FEN-F in acetonitrile.

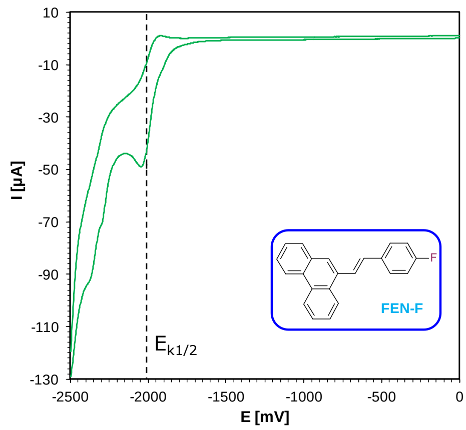

Figure S.55. Cyclic voltammetry of the reduction process for the compound FEN-F in acetonitrile.

Excitation and emission spectra for 9-[(E)-2 phenylethenyl]anthracene / 9-[(E)-2-phenylethenyl]phenanthrene derivatives in acetonitrile

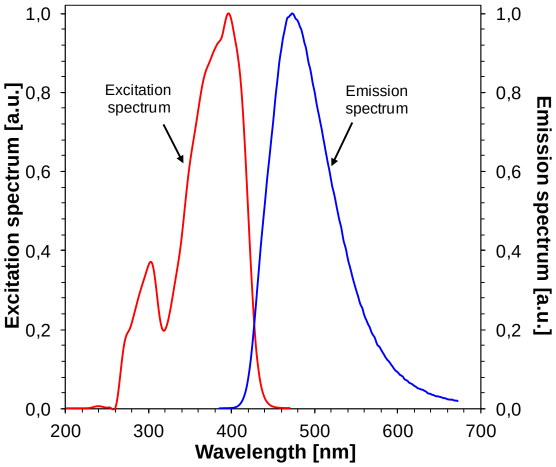

Figure S.56. Excitation and emission spectrum for compound ANT-H in acetonitrile.

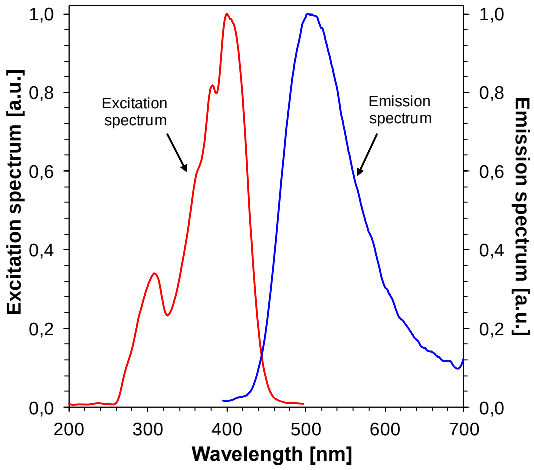

Figure S.57. Excitation and emission spectrum for compound ANT-CN in acetonitrile.

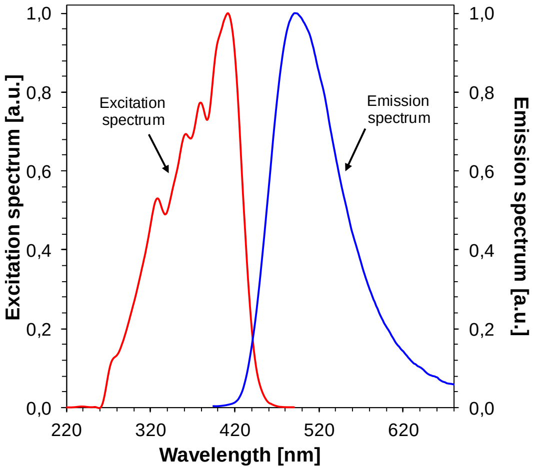

Figure S.58. Excitation and emission spectrum for compound ANT-SCH_3 in acetonitrile.

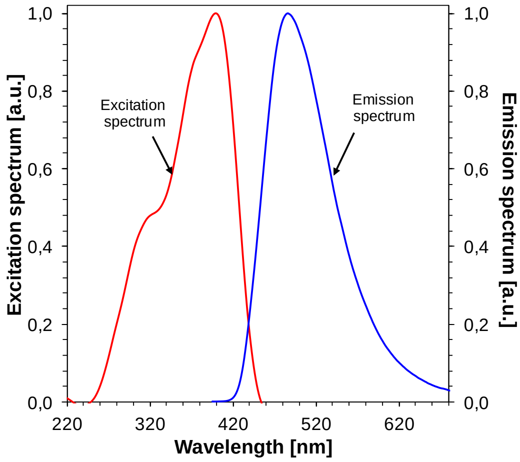

Figure S.59. Excitation and emission spectrum for compound ANT- C_6H_5 in acetonitrile.

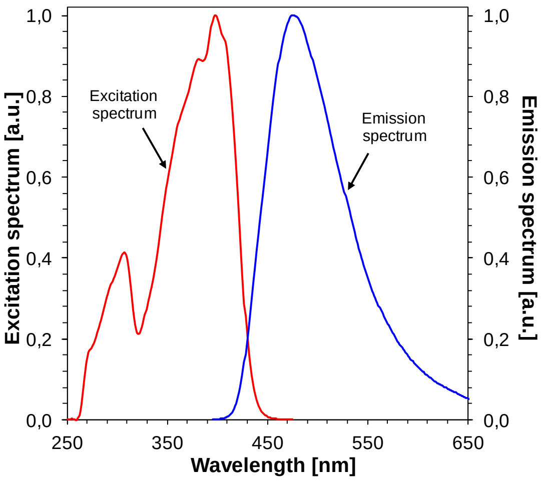

Figure S.60. Excitation and emission spectrum for compound ANT-CH_3 in acetonitrile.

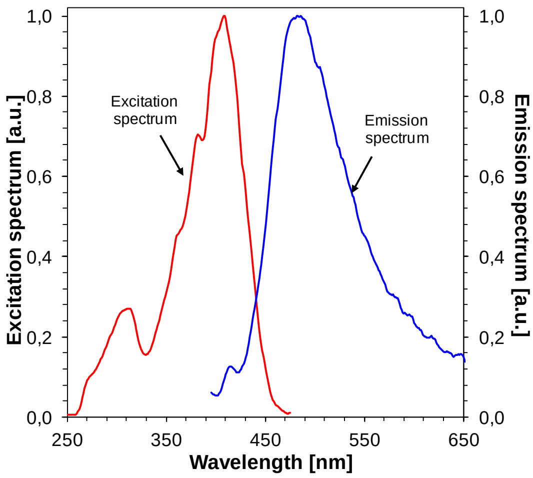

Figure S.61. Excitation and emission spectrum for compound ANT-OCH_3 in acetonitrile.

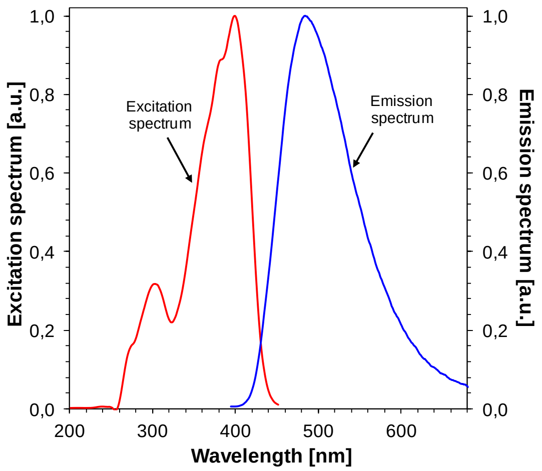

Figure S.62. Excitation and emission spectrum for compound ANT-PYR in acetonitrile.

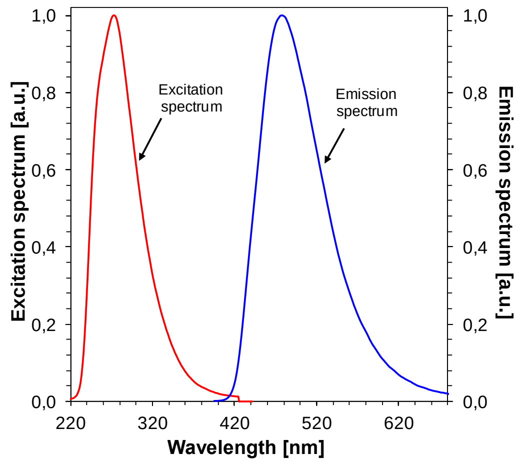

Figure S.63. Excitation and emission spectrum for compound ANT-Cl in acetonitrile.

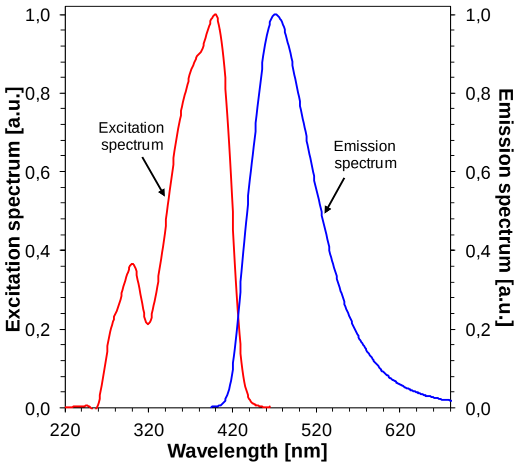

Figure S.64. Excitation and emission spectrum for compound ANT-F in acetonitrile.

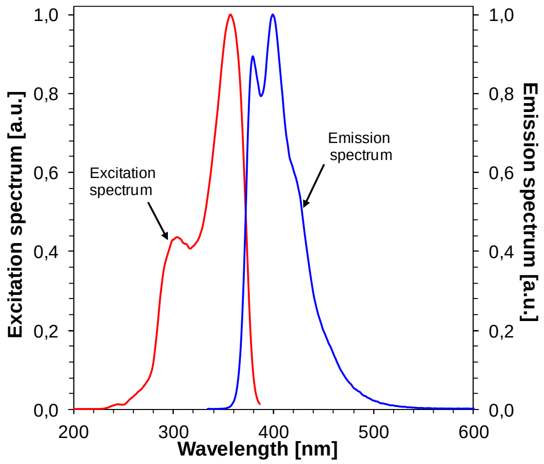

Figure S.65. Excitation and emission spectrum for compound FEN-H in acetonitrile.

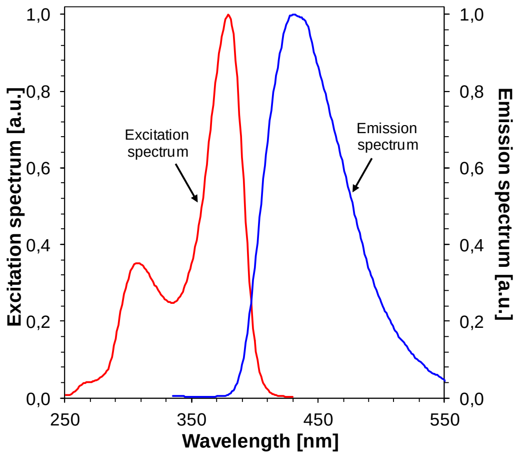

Figure S.66. Excitation and emission spectrum for compound FEN-CN in acetonitrile.

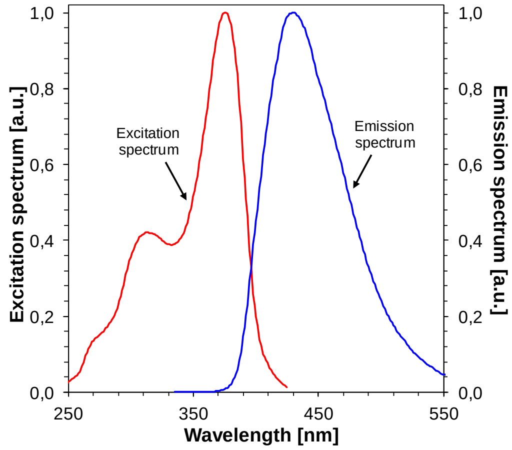

Figure S.67. Excitation and emission spectrum for compound FEN-SCH_3 in acetonitrile.

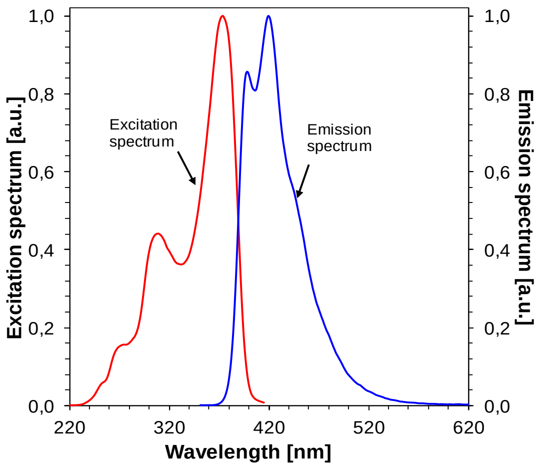

Figure S.68. Excitation and emission spectrum for compound FEN-C_6H_5 in acetonitrile.

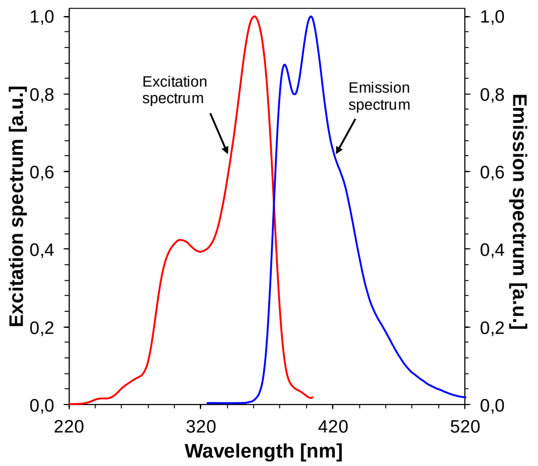

Figure S.69. Excitation and emission spectrum for compound FEN-CH_3 in acetonitrile.

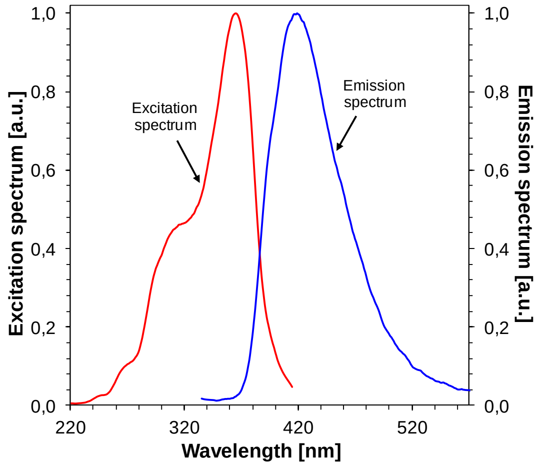

Figure S.70. Excitation and emission spectrum for compound FEN-OCH_3 in acetonitrile.

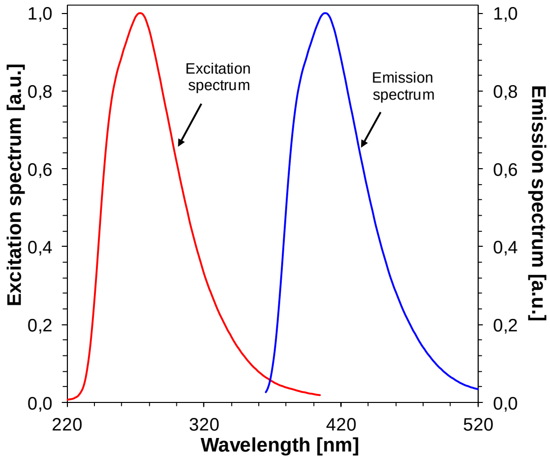

Figure S.71. Excitation and emission spectrum for compound FEN-PYR in acetonitrile.

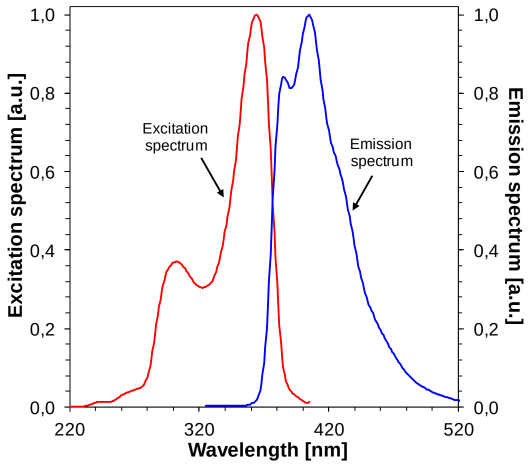

Figure S.72. Excitation and emission spectrum for compound FEN-Cl in acetonitrile.

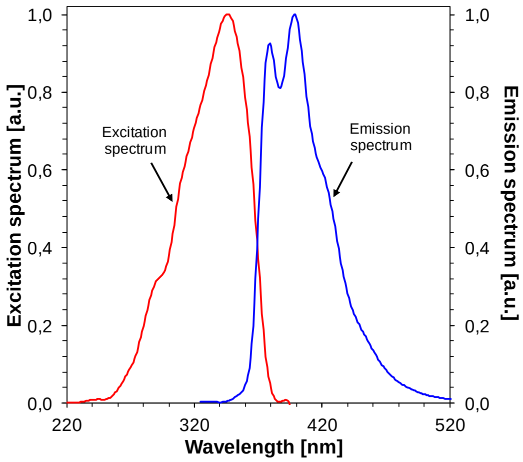

Figure S.73. Excitation and emission spectrum for compound FEN-F in acetonitrile.

Fluorescence quenching of investigated 9-[(E)-2 phenylethenyl]anthracene / 9-[(E)-2-phenylethenyl]phenanthrene derivatives with SpeedCure 938 with Stern-Volmer correlation

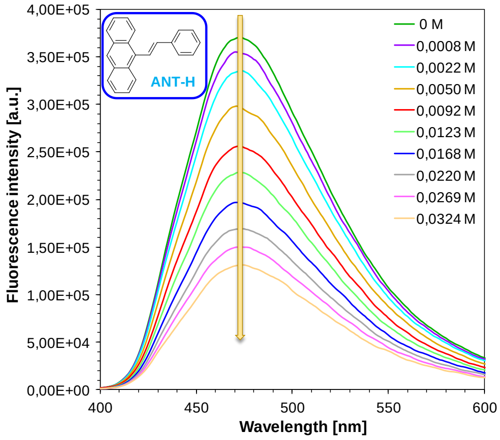

Figure S.74. Fluorescence quenching of compound ANT-H using SpeedCure 938 iodonium salt in acetonitrile.

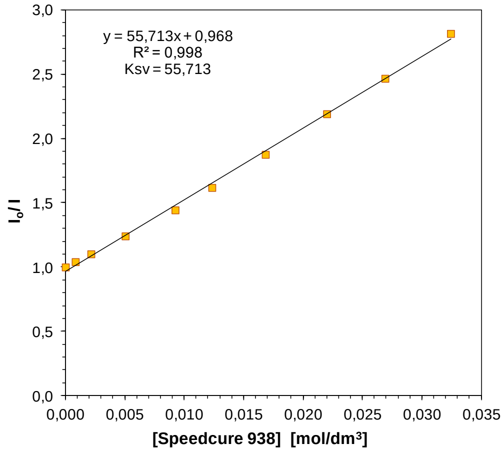

Figure S.75. Stern-Volmer correlation for compound ANT-H in the presence of SpeedCure 938 iodonium salt as a quencher.

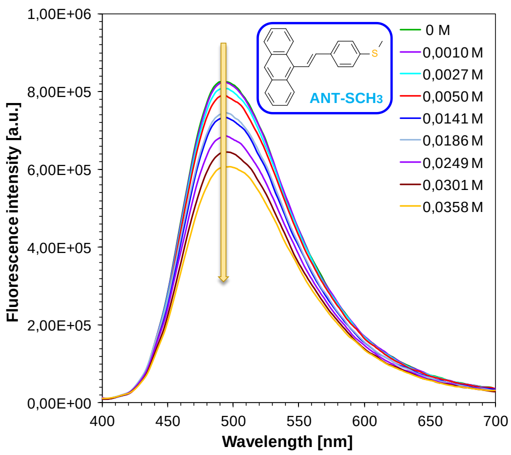

Figure S.76. Fluorescence quenching of compound ANT-SCH_3 using SpeedCure 938 iodonium salt in acetonitrile.

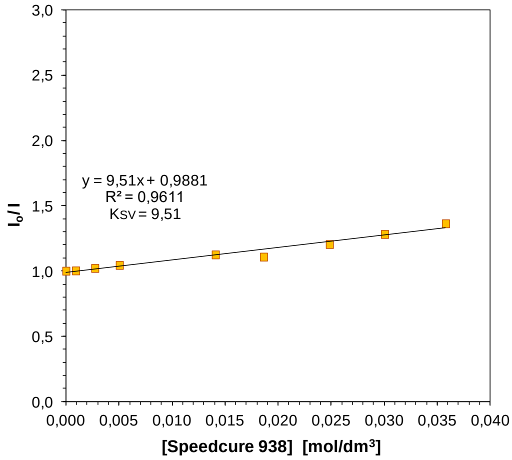

Figure S.77. Stern-Volmer correlation for compound ANT-SCH_3 in the presence of SpeedCure 938 iodonium salt as a quencher.

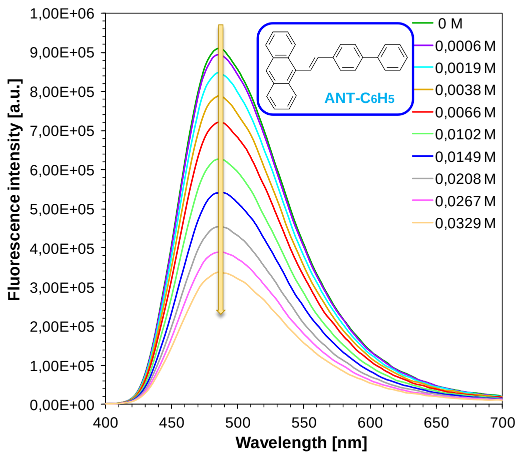

Figure S.78. Fluorescence quenching of compound ANT-C_6H_5 using SpeedCure 938 iodonium salt in acetonitrile.

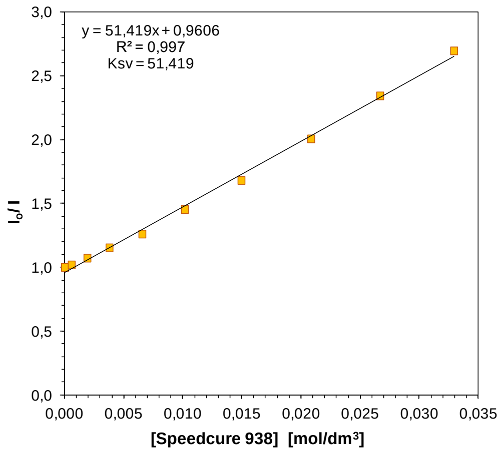

Figure S.79. Stern-Volmer correlation for compound ANT-C_6H_5 in the presence of SpeedCure 938 iodonium salt as a quencher.

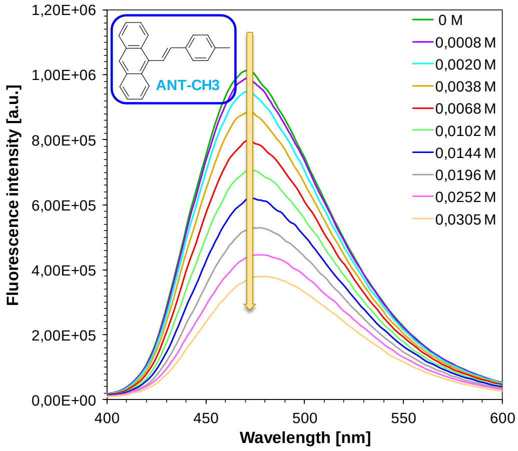

Figure S.80. Fluorescence quenching of compound ANT-CH_3 using SpeedCure 938 iodonium salt in acetonitrile.

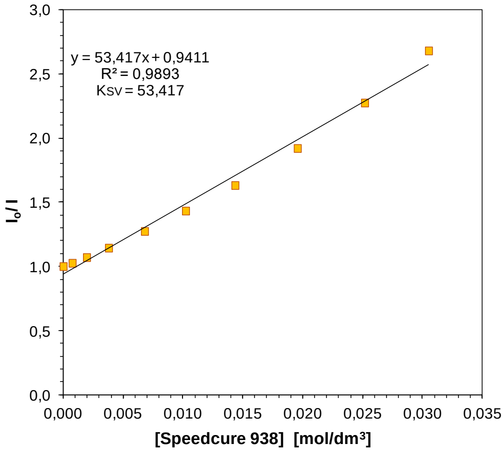

Figure S.81. Stern-Volmer correlation for compound ANT-CH_3 in the presence of SpeedCure 938 iodonium salt as a quencher.

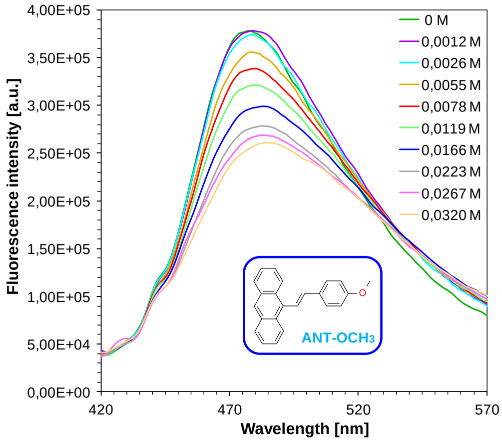

Figure S.82. Fluorescence quenching of compound ANT-OCH_3 using SpeedCure 938 iodonium salt in acetonitrile.

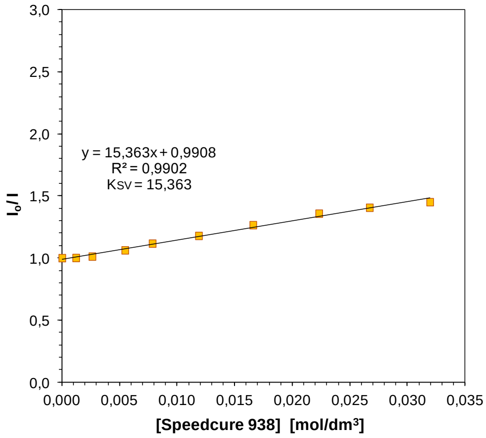

Figure S.83. Stern-Volmer correlation for compound ANT-OCH_3 in the presence of SpeedCure 938 iodonium salt as a quencher.

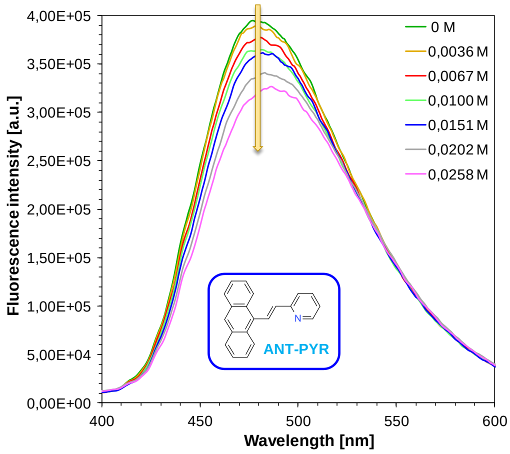

Figure S.84. Fluorescence quenching of compound ANT-PYR using SpeedCure 938 iodonium salt in acetonitrile.

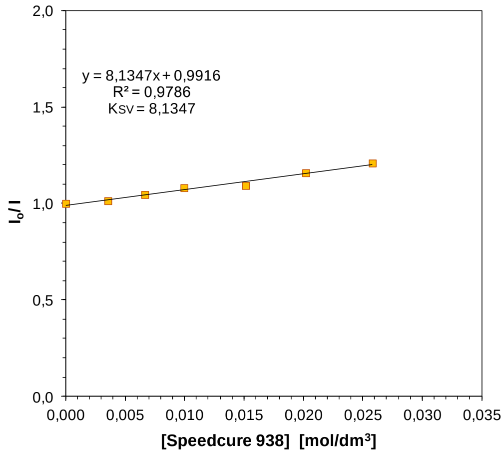

Figure S.85. Stern-Volmer correlation for compound ANT-PYR in the presence of SpeedCure 938 iodonium salt as a quencher.

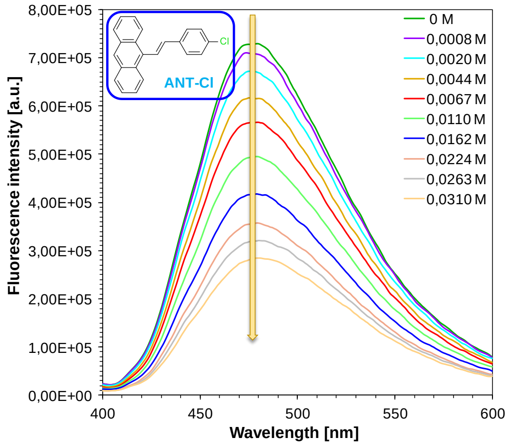

Figure S.86. Fluorescence quenching of compound ANT-Cl using SpeedCure 938 iodonium salt in acetonitrile.

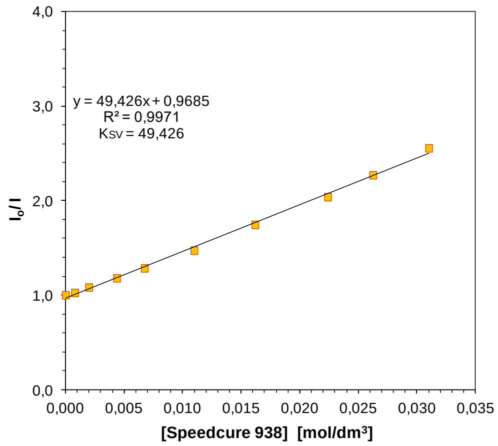

Figure S.87. Stern-Volmer correlation for compound ANT-Cl in the presence of SpeedCure 938 iodonium salt as a quencher.

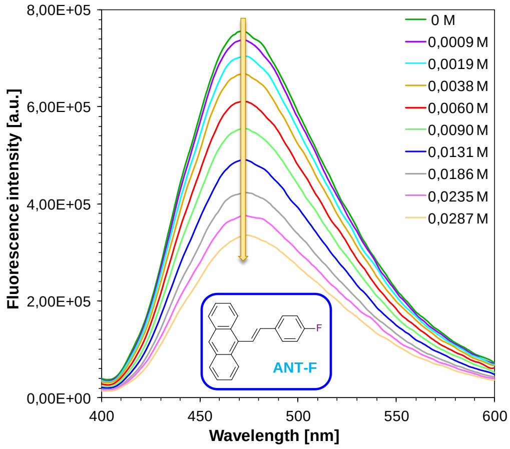

Figure S.88. Fluorescence quenching of compound ANT-F using SpeedCure 938 iodonium salt in acetonitrile.

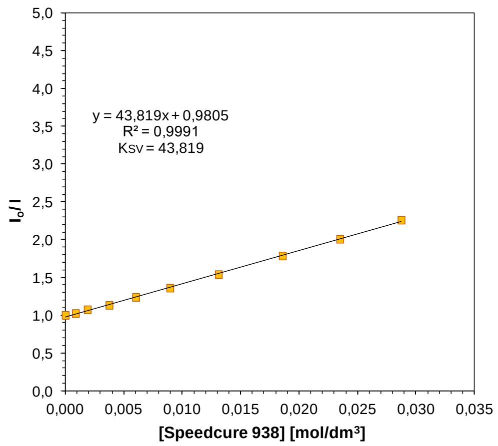

Figure S.89. Stern-Volmer correlation for compound ANT-F in the presence of SpeedCure 938 iodonium salt as a quencher.

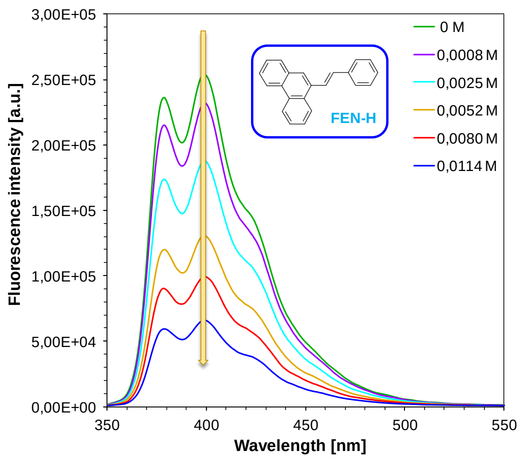

Figure S.90. Fluorescence quenching of compound FEN-H using SpeedCure 938 iodonium salt in acetonitrile.

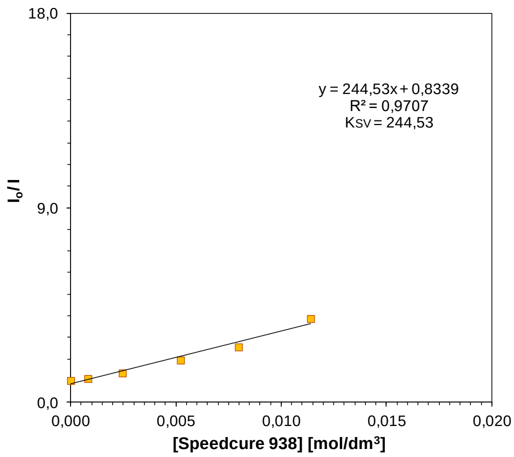

Figure S.91. Stern-Volmer correlation for compound FEN-H in the presence of SpeedCure 938 iodonium salt as a quencher.

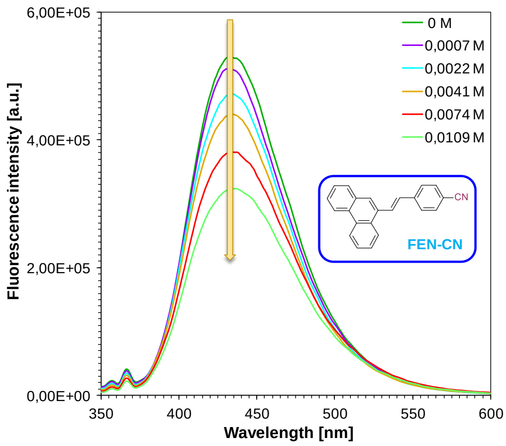

Figure S.92. Fluorescence quenching of compound FEN-CN using SpeedCure 938 iodonium salt in acetonitrile.

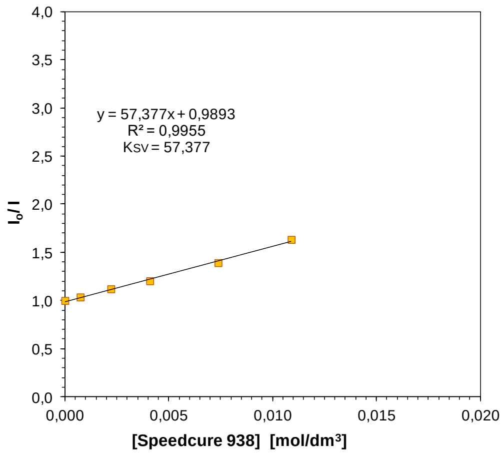

Figure S.93. Stern-Volmer correlation for compound FEN-CN in the presence of SpeedCure 938 iodonium salt as a quencher.

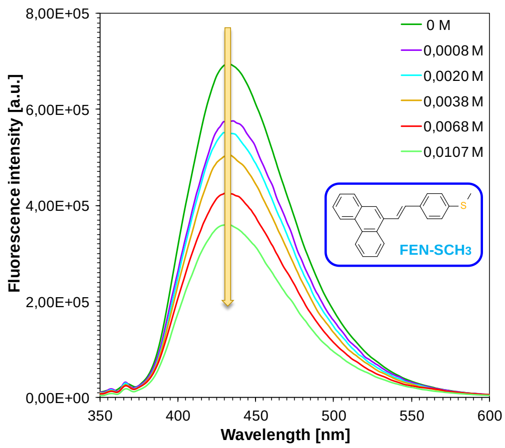

Figure S.94. Fluorescence quenching of compound FEN-SCH_3 using SpeedCure 938 iodonium salt in acetonitrile.

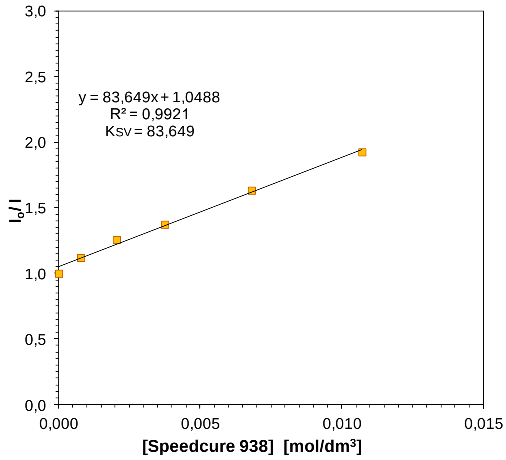

Figure S.95. Stern-Volmer correlation for compound FEN-SCH_3 in the presence of SpeedCure 938 iodonium salt as a quencher.

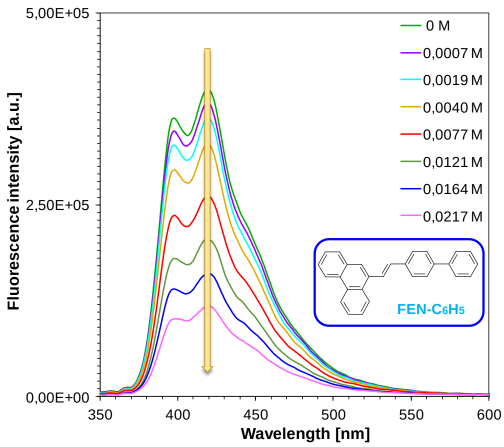

Figure S.96. Fluorescence quenching of compound FEN-C_6H_5 using SpeedCure 938 iodonium salt in acetonitrile.

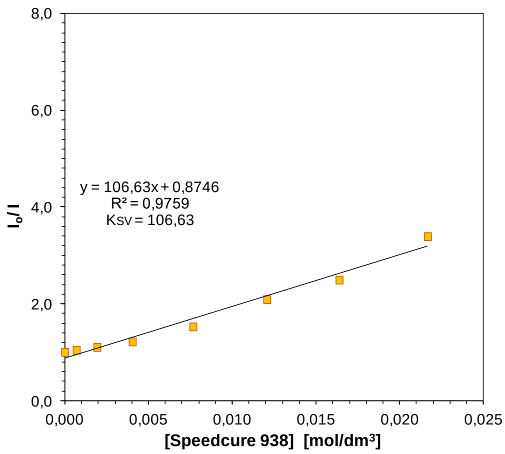

Figure S.97. Stern-Volmer correlation for compound FEN-C_6H_5 in the presence of SpeedCure 938 iodonium salt as a quencher.

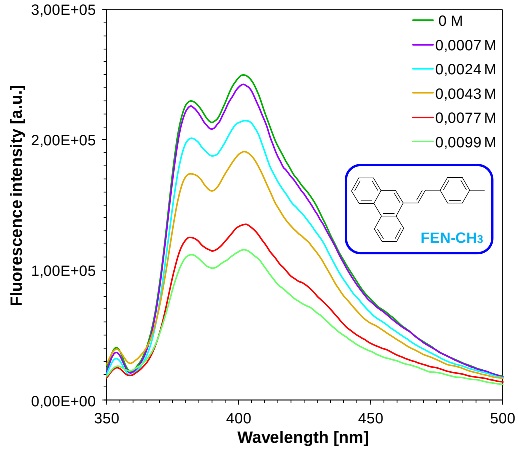

Figure S.98. Fluorescence quenching of compound FEN-CH_3 using SpeedCure 938 iodonium salt in acetonitrile.

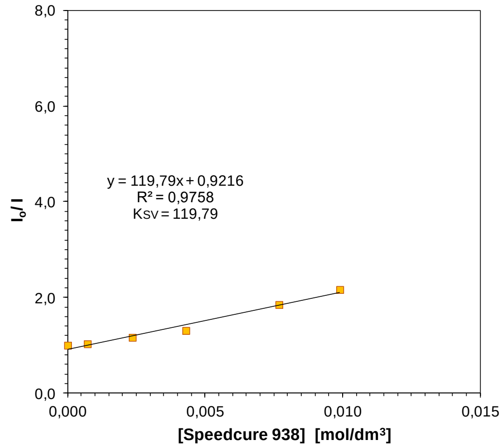

Figure S.99. Stern-Volmer correlation for compound FEN-CH_3 in the presence of SpeedCure 938 iodonium salt as a quencher.

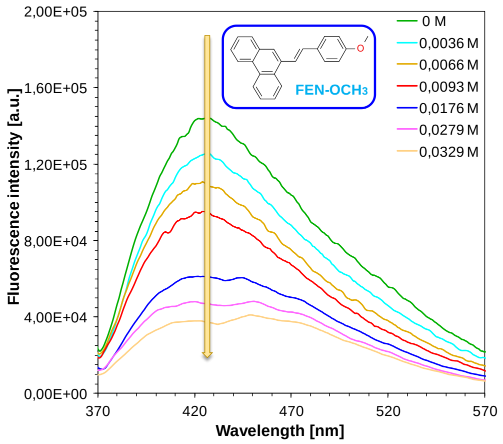

Figure S.100. Fluorescence quenching of compound FEN-OCH_3 using SpeedCure 938 iodonium salt in acetonitrile.

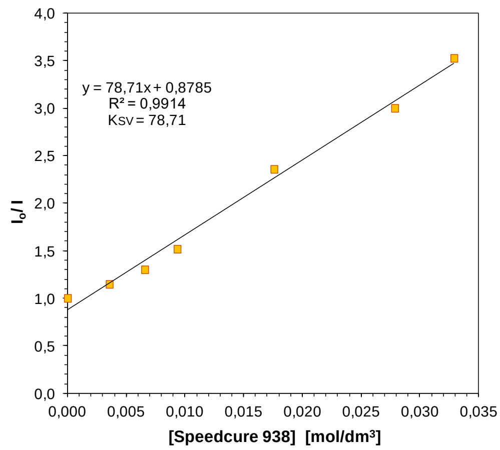

Figure S.101. Stern-Volmer correlation for compound FEN-OCH_3 in the presence of SpeedCure 938 iodonium salt as a quencher.

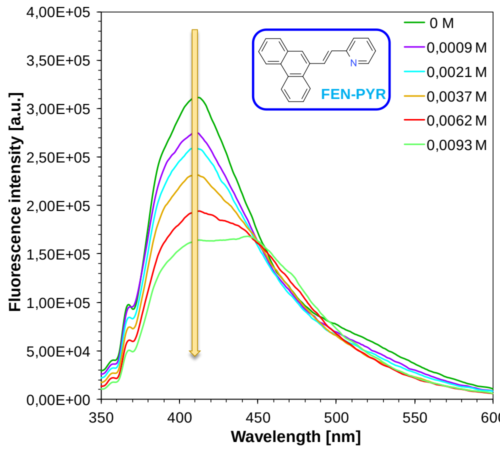

Figure S.102. Fluorescence quenching of compound FEN-PYR using SpeedCure 938 iodonium salt in acetonitrile.

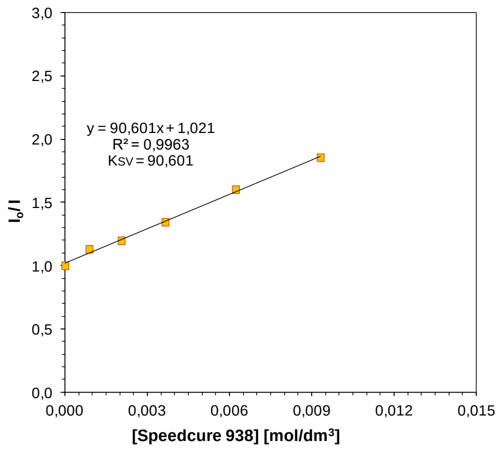

Figure S.103. Stern-Volmer correlation for compound FEN-PYR in the presence of SpeedCure 938 iodonium salt as a quencher.

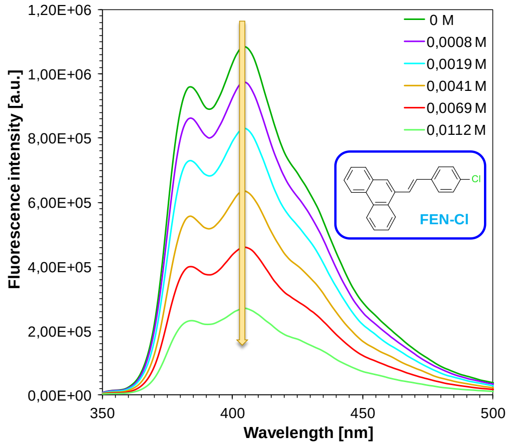

Figure S.104. Fluorescence quenching of compound FEN-Cl using SpeedCure 938 iodonium salt in acetonitrile.

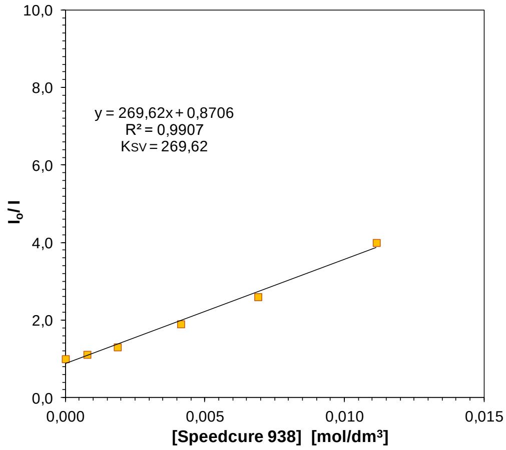

Figure S.105. Stern-Volmer correlation for compound FEN-Cl in the presence of SpeedCure 938 iodonium salt as a quencher.

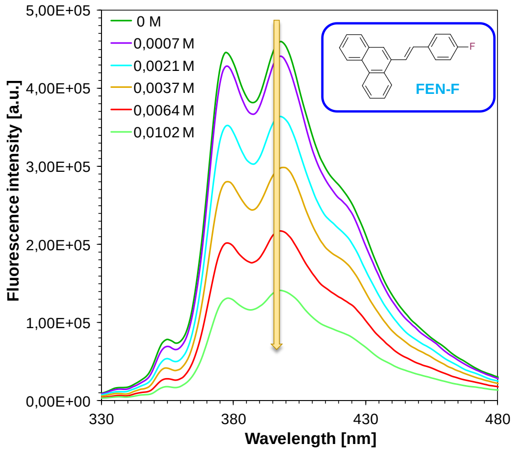

Figure S.106. Fluorescence quenching of compound FEN-F using SpeedCure 938 iodonium salt in acetonitrile.

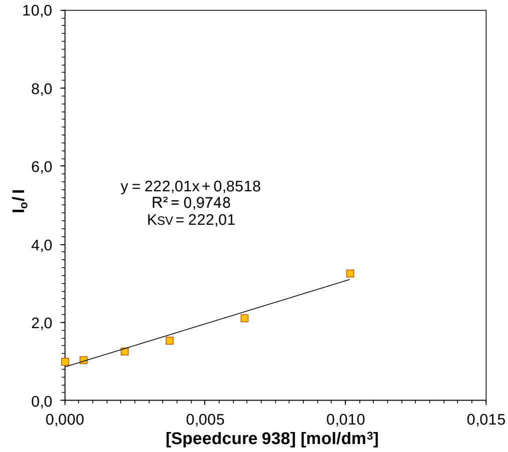

Figure S.107. Stern-Volmer correlation for compound FEN-F in the presence of SpeedCure 938 iodonium salt as a quencher.

Investigation of the electron transfer mechanism between 9-[(*E*)-2 phenylethenyl]anthracene derivatives / 9-[(*E*)-2-phenylethenyl]phenanthrene derivatives and the iodonium salt SpeedCure 938

Based on emission and excitation measurements, which made it possible to determine the energy of singlet states, and based on the determined oxidation potential it was possible to determine the Gibbs free energy. The Rehm-Weller equation was used for this purpose:

$$\Delta G_{et} = F[E_{ox}(D/D^{\cdot+}) - E_{red}(A^{\cdot-}/A)] - E_{00} - Ze^2/\varepsilon a$$ [10,11]

$E_{ox}(D/D^{\cdot+})$ – oxidation potential of the photosensitizer (determined electrochemically)

$E_{red}(A^{\cdot-}/A)$ – electron acceptor reduction potential (electrochemically determined),

(-0.68 V value for diaryliodonium salt (vs. SCE))

E_{00} – The singlet state energy of the photosensitizer determined from the excitation and emission spectra

$Ze^2/\varepsilon a$ - interaction energy for the initially formed ion pair, negligible in polar solvents

Obtaining negative Gibbs free energy values confirmed the possibility of electron transfer between the 9-[(*E*)-2-phenylethenyl]anthracene / 9-[(*E*)-2-phenylethenyl]phenantrene derivatives in the excited state and the iodonium salt in the ground state. Subsequently, fluorescence quenching of the tested compounds was performed using a quencher as diphenyliodonium salt SpeedCure 938. It was observed that SpeedCure 938 causes a decrease in the fluorescence intensity of the tested compounds. Based on the carried out measurements, Stern-Volmer K_{SV} correlation was determined.

Due to the fluorescence quenching measurements performed, it was also possible to determine the electron transfer rate constant between the photosensitizer in the excited state and the diphenyliodonium salt. The electron transfer constant (kq) was determined from Stern-Volmer equation:

$$I_0/I = 1 + K_{SV}[\text{SpeedCure 938}] = 1 + kq\tau_0[\text{SpeedCure 938}]$$ [12,13]

I_0 - fluorescence intensity of the photosensitizer (anthracene/phenanthrene derivatives) in the absence of fluorescence quencher (SpeedCure 938 iodonium salt)

I - fluorescence intensity of the photosensitizer (anthracene/phenanthrene derivatives) in the presence of fluorescence quencher (SpeedCure 938 iodonium salt)

τ_0 – excited-state lifetime of photosensitizer (anthracene/phenanthrene derivatives) in the absence of fluorescence quencher (SpeedCure 938 iodonium salt)

The final step in studying the mechanism was to determine the quantum yield of electron transfer from the excited state:

$$\boldsymbol{\Phi et(S1)} = \frac{\mathbf{K_{SV}\,[SpeedCure\ 938]}}{\mathbf{1 + K_{SV}\,[SpeedCure\ 938]}}$$

Cationic photopolymerization of epoxy monomer CADE, UV-LED @365 nm

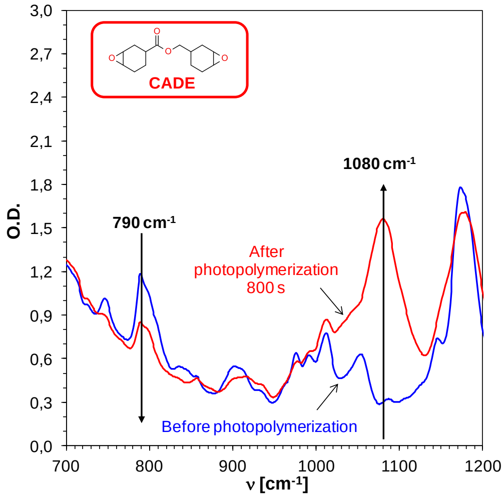

Figure S.108. FT-IR spectrum changes during cationic photopolymerization of epoxy monomer CADE

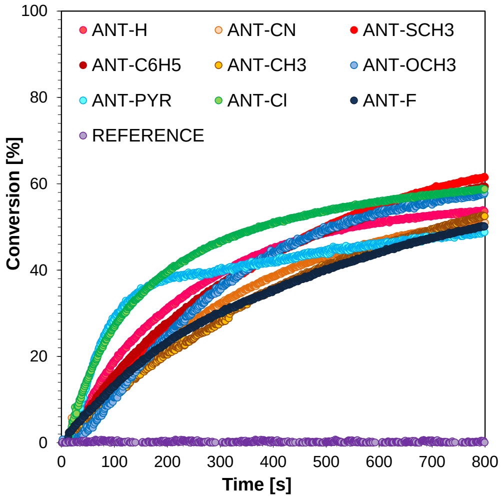

(a)

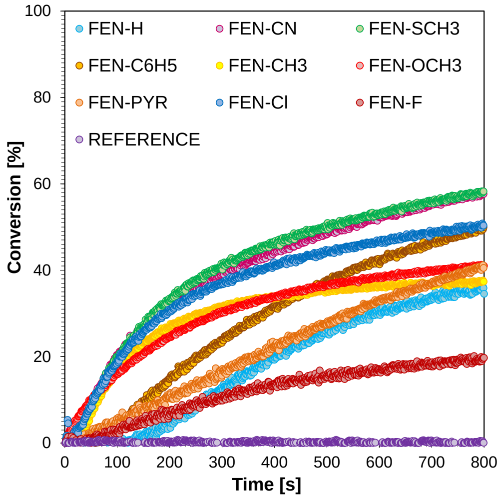

(b)

Figure S.109. Kinetic profiles obtained during the cationic photopolymerization of a CADE epoxy monomer for bimolecular photoinitiating systems based on studied compounds and iodonium salt SpeedCure 938; radiation source - a diode emitting radiation at a wavelength of 365 nm, (a) 9-[(E)-2-phenylethenyl]anthracene derivatives as photosensitizers, (b) 9-[(E)-2-phenylethenyl]phenantrene derivatives as photosensitizers.

REFERENCE: IOD (1% w/w) and epoxy monomer CADE without photosensitizers.

Cationic photopolymerization of epoxy monomer CADE, VIS-LED @405 nm

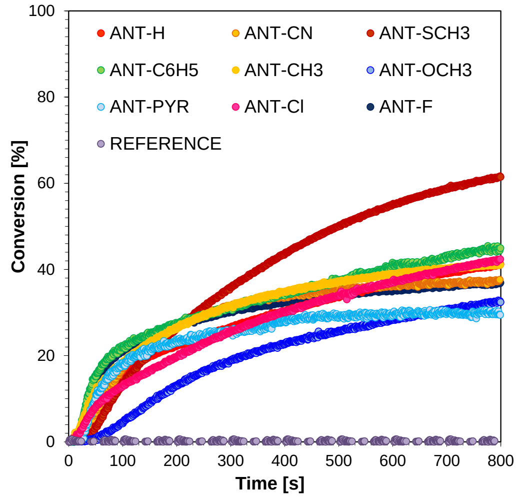

Figure S.110. Kinetic profiles obtained during the cationic photopolymerization of a CADE epoxy monomer for bimolecular photoinitiating systems based on 9-[€-2-phenylethenyl]anthracene derivatives as photosensitizers and iodonium salt SpeedCure 938; radiation source - a diode emitting radiation at a wavelength of 405 nm.

REFERENCE: IOD (1% w/w) and epoxy monomer CADE without photosensitizers.

Cationic photopolymerization of epoxy monomer CADE, Vis-LED @420 nm

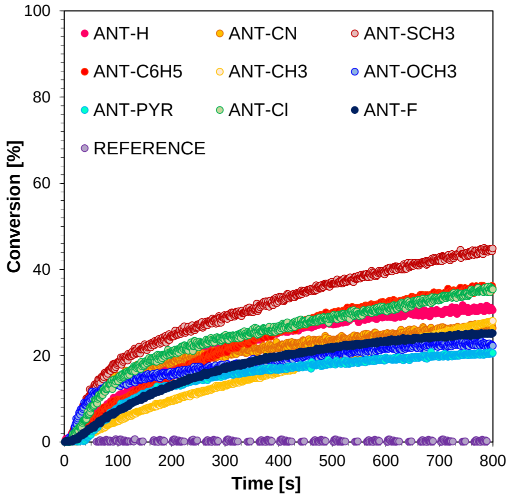

Figure S.111. Kinetic profiles obtained during the cationic photopolymerization of a CADE epoxy monomer for bimolecular photoinitiating systems based on 9-[(E)-2-phenylethenyl]anthracene derivatives as photosensitizers and iodonium salt SpeedCure 938; radiation source - a diode emitting radiation at a wavelength of 420 nm.

REFERENCE: IOD (1% w/w) and epoxy monomer CADE without photosensitizers.

Free-radical photopolymerization of acrylate monomer TMPTA, UV-LED @365 nm

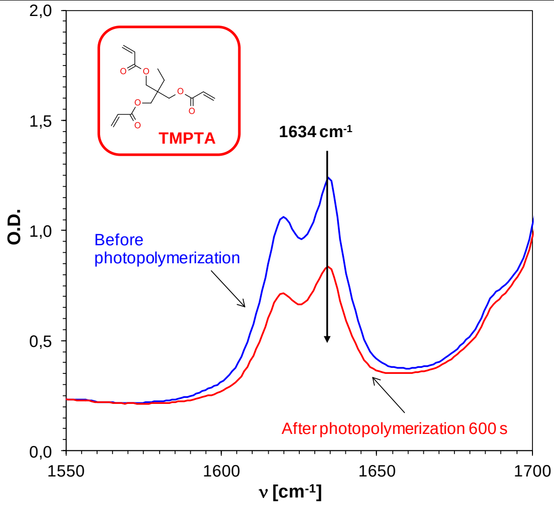

Figure S.112. FT-IR spectrum changes during free-radical photopolymerization of acrylate monomer TMPTA

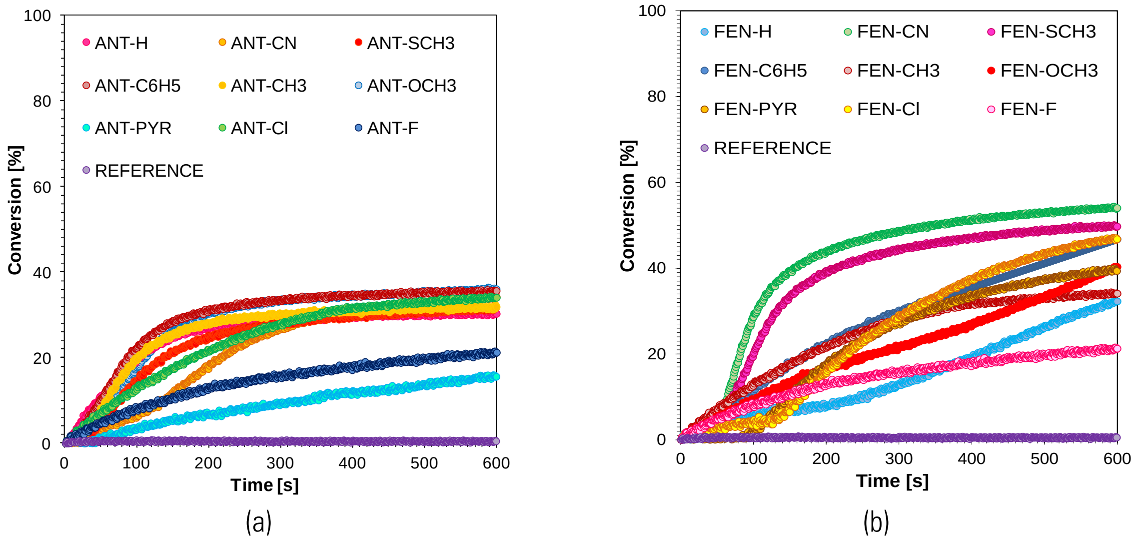

Figure S.113. Kinetic profiles obtained during the radical photopolymerization of a TMPTA acrylate monomer for bimolecular photoinitiating systems based on studied compounds and iodonium salt SpeedCure 938; radiation source - a diode emitting radiation at a wavelength of 365 nm, (a) 9-[(E)-2-phenylethenyl]anthracene derivatives as photosensitizers, (b) 9-[(E)-2-phenylethenyl]phenantrene derivatives as photosensitizers.

REFERENCE: IOD (1% w/w) and acrylate monomer TMPTA without photosensitizers.

Free-radical photopolymerization of acrylate monomer TMPTA, Vis-LED @405 nm

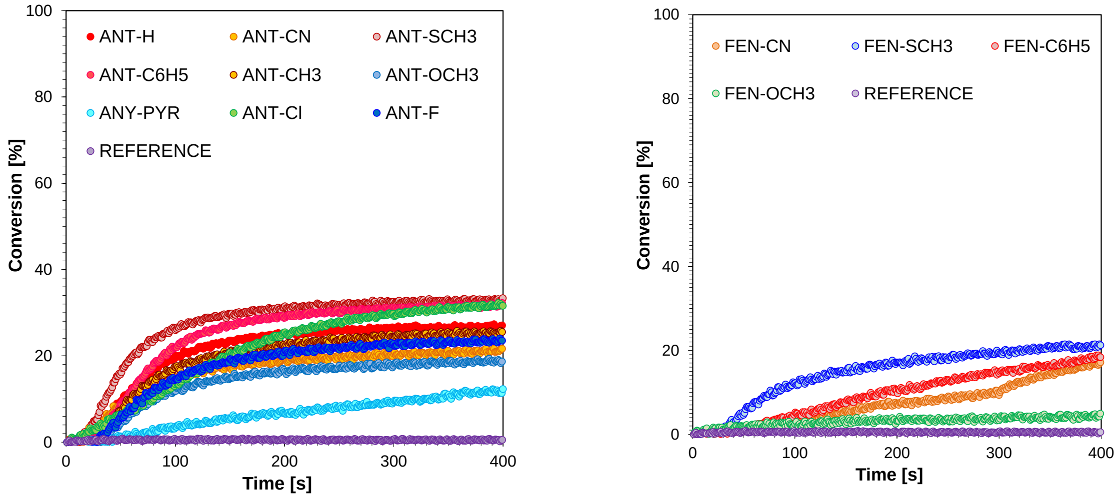

(a) (b)

Figure S.114. Kinetic profiles obtained during the radical photopolymerization of a TMPTA acrylate monomer for bimolecular photoinitiating systems based on studied compounds and iodonium salt SpeedCure 938; radiation source - a diode emitting radiation at a wavelength of 365 nm, (a) 9-[(E)-2-phenylethenyl]anthracene derivatives as photosensitizers, (b) 9-[(E)-2-phenylethenyl]phenantrene derivatives as photosensitizers.

REFERENCE: IOD (1% w/w) and acrylate monomer TMPTA without photosensitizers.

Free-radical photopolymerization of acrylate monomer TMPTA, Vis-LED @420 nm

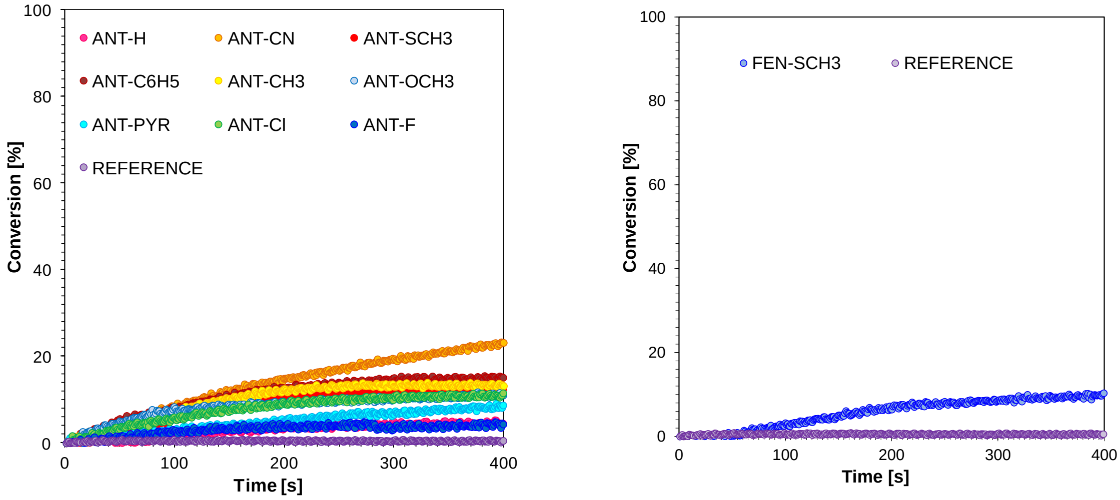

(a) (b)

Figure S.115. Kinetic profiles obtained during the radical photopolymerization of a TMPTA acrylate monomer for bimolecular photoinitiating systems based on studied compounds and iodonium salt SpeedCure 938; radiation source - a diode emitting radiation at a wavelength of 420 nm, (a) 9-[(E)-2-phenylethenyl]anthracene derivatives as photosensitizers, (b) 9-[(E)-2-phenylethenyl]phenantrene derivatives as photosensitizers.

REFERENCE: IOD (1% w/w) and acrylate monomer TMPTA without photosensitizers.

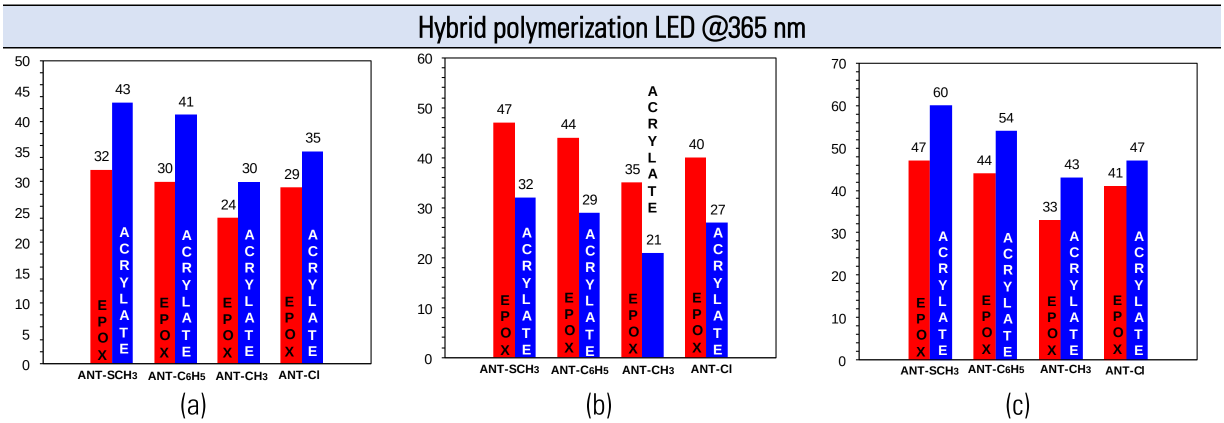

Figure S.116. Kinetic profiles obtained during the hybrid photopolymerization of CADE/TMPTA/M100 monomers for bimolecular photoinitiating systems based on different 9-[(E)-2-phenylethenyl]anthracene derivatives (ANT-SCH_3, ANT-C_6H_5, ANT-CH_3, ANT-Cl) and iodonium salt SpeedCure 938; radiation source - a diode emitting radiation at a wavelength of 365 nm (a) laminate condition, thin layer; (b) air thin layer; (c) laminate condition, thick layer.

Table 1. The values of acrylate and epoxy monomer conversion were obtained during hybrid photopolymerization using UV LED @365 nm during different experimental conditions.

Light source: LED @365 nm							
Composition	**Experimental conditions**	**Thickness**	**Monitoring wavelengths**	**Functional group conversion**			
				ANT-SCH_3	**ANT-C_6H_5**	**ANT-CH_3**	**ANT-Cl**
CADE/TMPTA/M100 (2/2/1 w/w/w)	Laminate	25 µm	EPOX at 790 cm^{-1}	32	30	24	29
			ACRYLATE at 1,635 cm^{-1}	43	41	30	35
	Air thin layer	25 µm	EPOX at 790 cm^{-1}	47	44	35	40
			ACRYLATE at 1,635 cm^{-1}	32	29	21	27
	Air thick layer	1,16 mm	EPOX at 3,700 cm^{-1}	47	44	33	41
			ACRYLATE at 6,165 cm^{-1}	60	54	43	47

Hybrid polymerization (various nanofillers)

2.65 mW/cm²

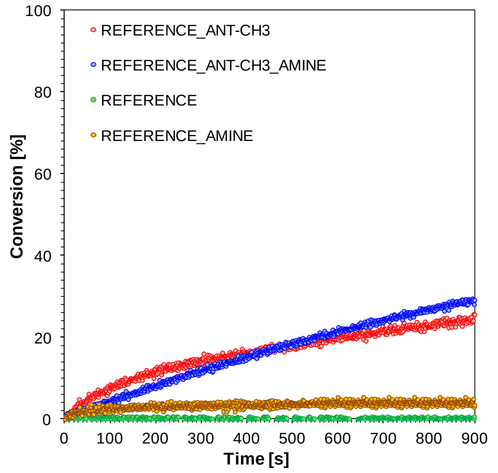

(a)

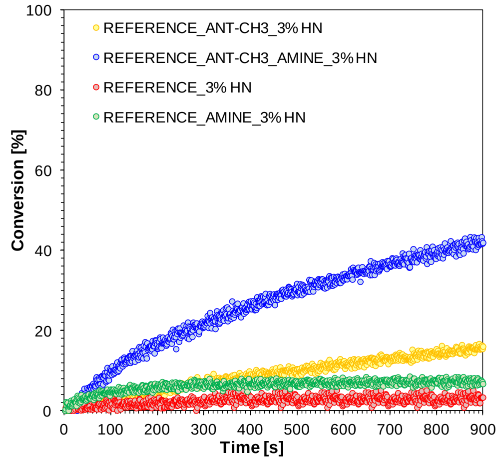

(b)

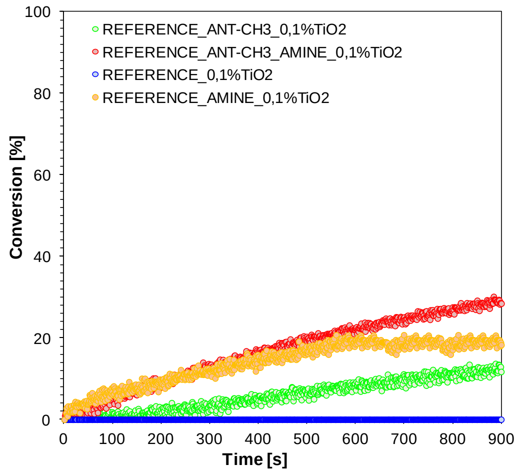

(c)

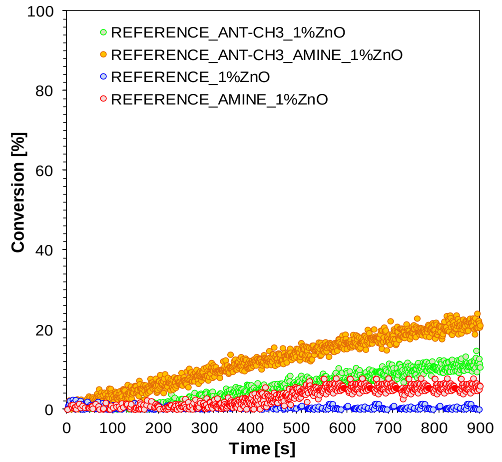

(d)

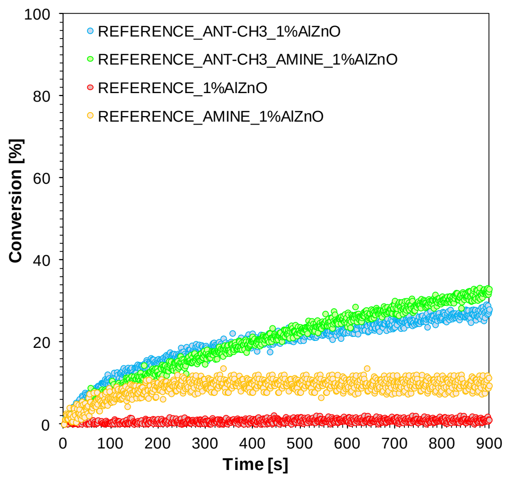

(e)

Figure S.117. Kinetic profiles obtained during the hybrid photopolymerization of HEMA/BEDA monomers for bimolecular photoinitiating systems based on different 9-[(E)-2-phenylethenyl]anthracene derivative (ANT-CH_3) and iodonium salt SpeedCure 938; radiation source - a diode emitting radiation at a wavelength of 405 nm (2.65 mW/cm^2) (a) without nanofillers, (b) 3% Halloysite nanoclay, (c) 0,1 % TiO_2, (d) 1 % ZnO, (e) 1 % AlZnO.

REFERENCE: IOD (1% w/w) and acrylate monomer BEDA and methacrylate monomer HEMA (7/3) without photosensitizers.

26.50 mW/cm^2

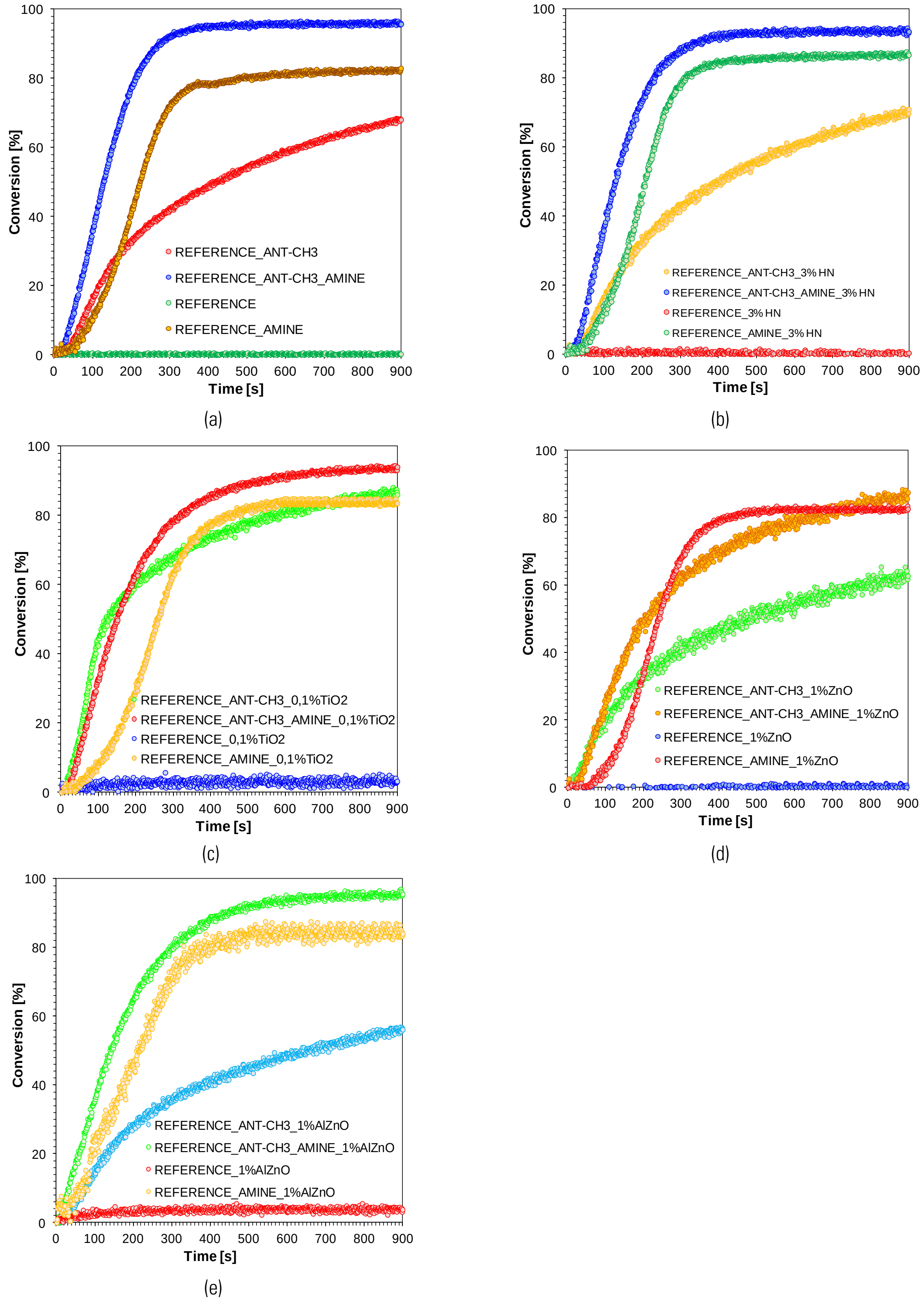

Figure S.118. Kinetic profiles obtained during the hybrid photopolymerization of HEMA/BEDA monomers for bimolecular photoinitiating systems based on different 9-[(E)-2-phenylethenyl]anthracene derivative (ANT-CH_3) and iodonium salt SpeedCure 938; radiation source - a diode emitting radiation at a wavelength of 405 nm (26.50 mW/cm^2) (a) without nanofillers, (b) 3% Halloysite nanoclay, (c) 0,1 % TiO_2, (d) 1 % ZnO, (e) 1 % AlZnO.

REFERENCE: IOD (1% w/w) and acrylate monomer BEDA and methacrylate monomer HEMA (7/3) without photosensitizers.

3D printouts

ANT-H, IOD (0.1/1 w/w), CADE/TMPTA/M100 (2/2/1)

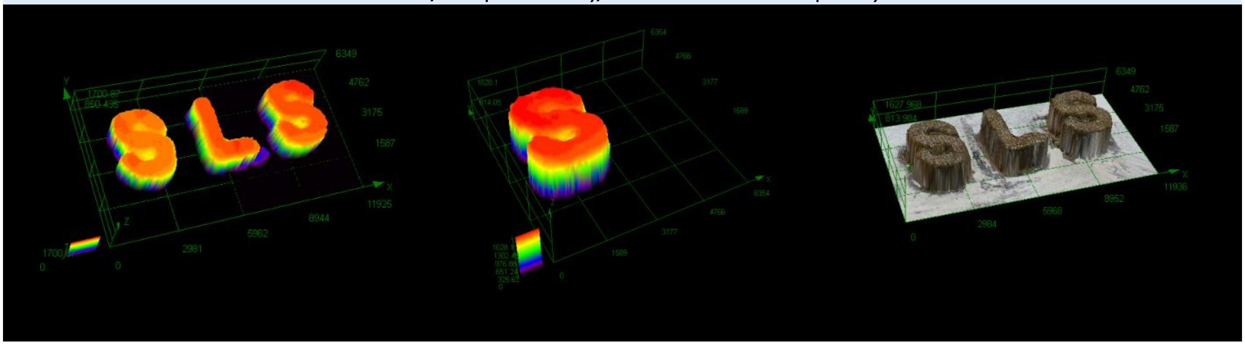

ANT-CN, IOD (0.1/1 w/w), CADE/TMPTA/M100 (2/2/1)

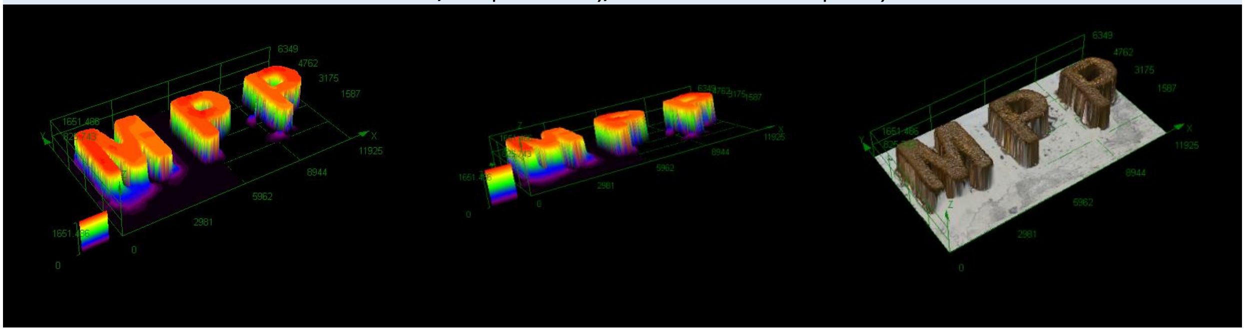

ANT-SCH_3, IOD (0.1/1 w/w), CADE/TMPTA/M100 (2/2/1)

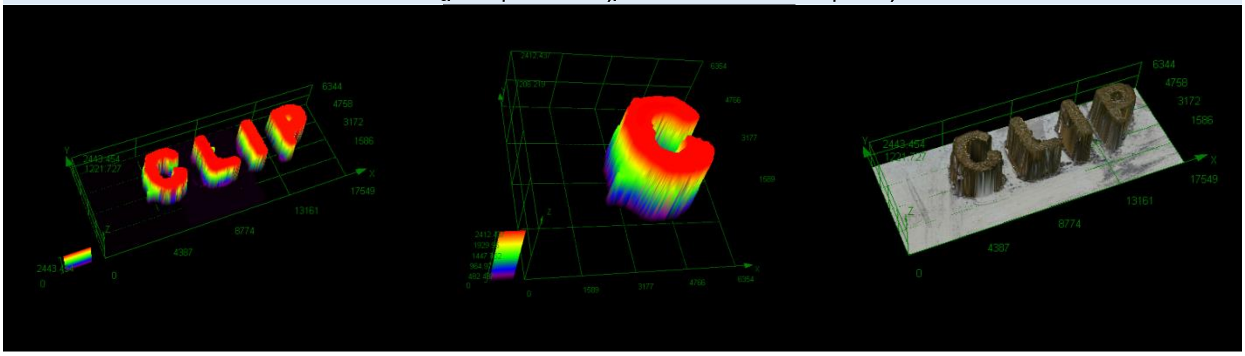

ANT-C_6H_5, IOD (0.1/1 w/w), CADE/TMPTA/M100 (2/2/1)

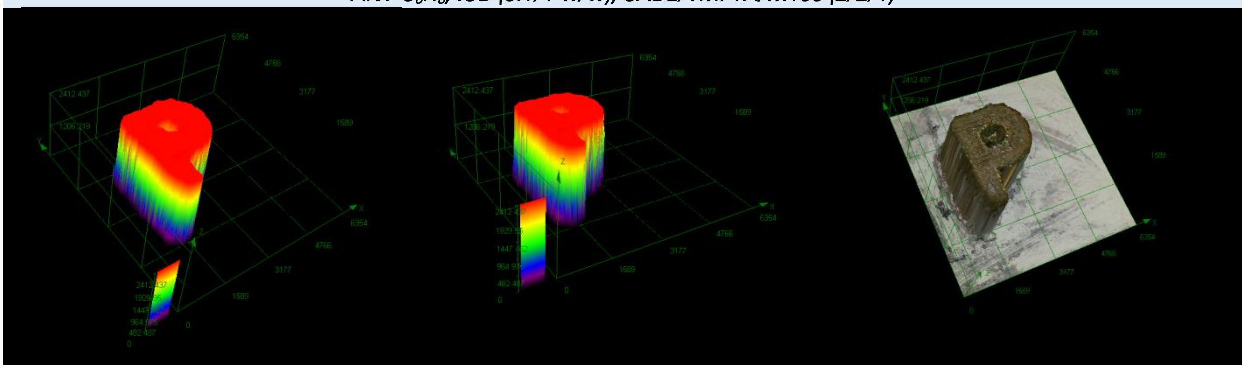

ANT-OCH_3, IOD (0.1/1 w/w), CADE/TMPTA/M100 (2/2/1)

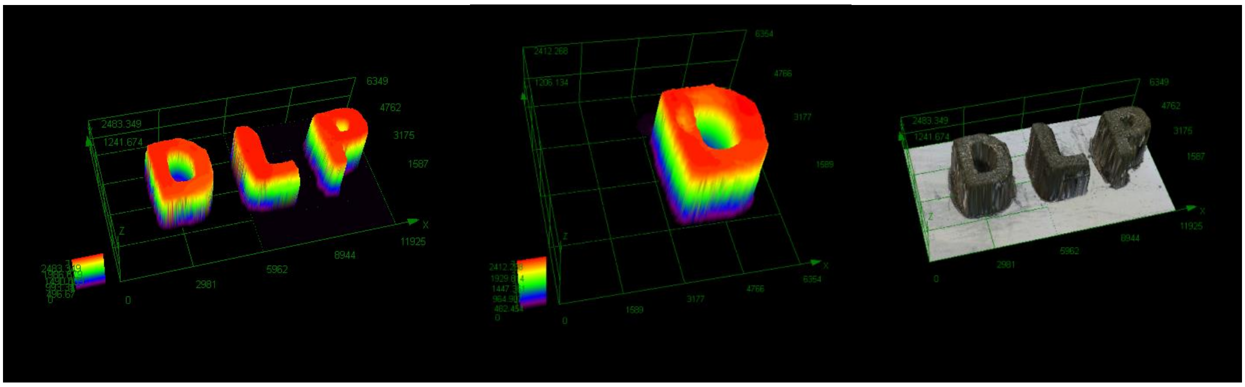

ANY-PYR, IOD (0.1/1 w/w), CADE/TMPTA/M100 (2/2/1)

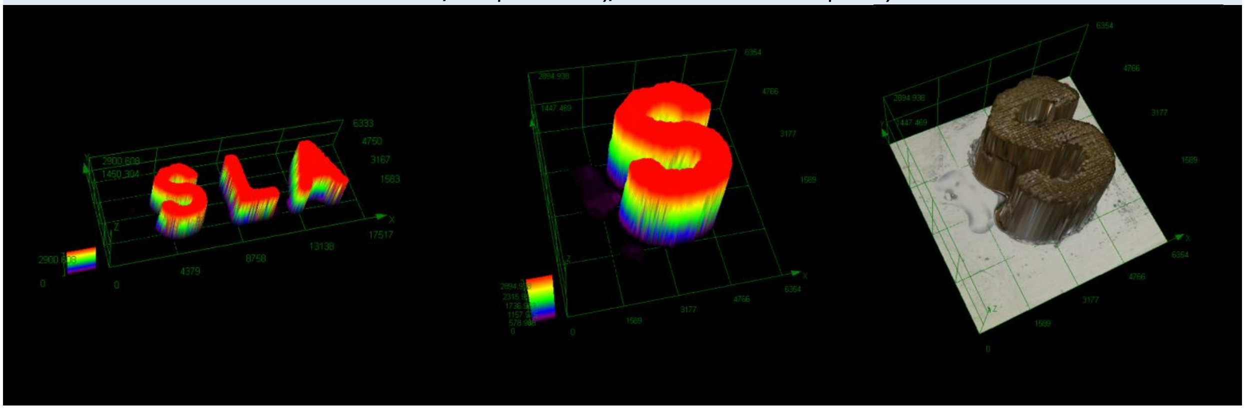

ANT-Cl, IOD (0.1/1 w/w), CADE/TMPTA/M100 (2/2/1)

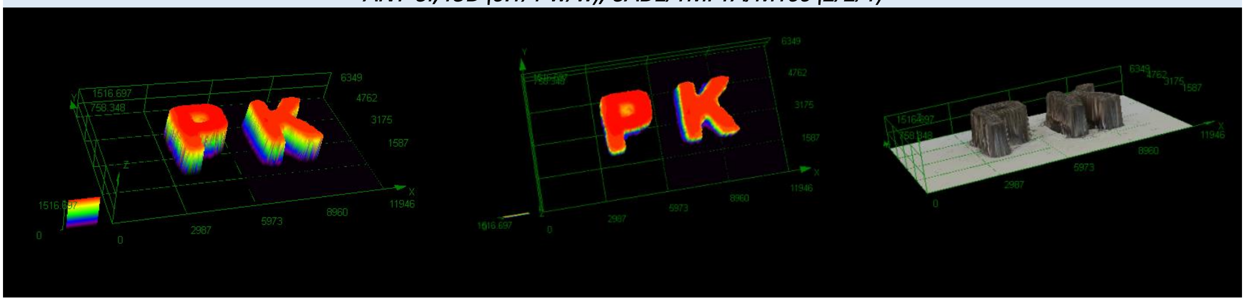

ANT-F, IOD (0.1/1 w/w), CADE/TMPTA/M100 (2/2/1)

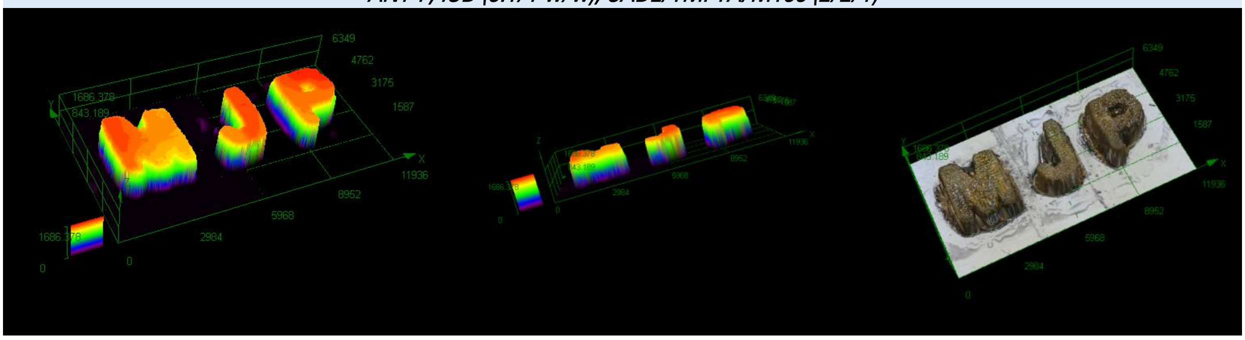

Photo 1. Photographs of a 3D printout obtained from a hybrid (CADE/TMPTA/M100) composition based on different 9-[(E)-2-phenylethenyl]anthracene derivatives.

REFERENCES

1 T. Ismail, S. Shafi, J. Srinivas, D. Sarkar, Y. Qurishi, J. Khazir, M. Sarwar, H. Mahabalarao and S. Kumar, *Bioorg. Chem.*, 2016, **64**, 97–102.
2 A. Link, C. Fischer and C. Sparr, 2015, 12163–12166.
3 N. Zhou, J. Wang, J. Huang, S. Luo and X. Shao, *Opt. Mater. (Amst).*, 2021, **113**, 110832.
4 S. Pratihar, A. Bhattacharyya and E. Prasad, *J. Photochem. Photobiol. A Chem.*, 2020, **396**, 112458.
5 G. Gurzadyan; H. Gorner, *Chem. Phys. Lett.*, 2002, **359**, 146–152.
6 E. J. Shin, R. Stackow, C. S. Foote, L. Angeles and S. Korea, *Phys. Chem. Chem. Phys.*, 2002, **4**, 5088–5095.
7 K. P. K. K.C. Kumara Swamy, V. Srinivas, K.V.P. Pavan Kumar, *Synthesis (Stuttg).*, 2007, **2007**, 893–901.
8 Abdol R. Hajipour; F. Rafiee, *J. organometalic Chem.*, 2011, **696**, 2669–2675.
9 A. Milián, P. Garcia-Garcia, A. Perez-Redondo, R. Sanz, J. J. Vaquero and M. A. Fernández-Rodriguez, *Org. Lett.*, 2020, **22**, 8464–8469.
10 W. Tomal, D. Krok, A. Chachaj-Brekiesz and J. Ortyl, *Eur. Polym. J.*, 2021, **156**, 110603.
11 M. Narayanan, G. Kodali, V. R. Singh, V. Velvadapu and R. J. Stanley, *J. Photochem. Photobiol. A Chem.*, 2012, **249**, 9–14.
12 M. H. Gehlen, *J. Photochem. Photobiol. C Photochem. Rev.*, 2020, **42**, 100338.
13 H. S. Geethanjali, D. Nagaraja, R. M. Melavanki and R. A. Kusanur, *J. Lumin.*, 2015, **167**, 216–221.